ESD-TR-71-246

July 1971

MODIFIED DIPOLES : I

THEORETICAL AND EXPERIMENTAL STUDY

FINAL SUMMARY REPORT

Prepared by

Harvard University

Cambridge, Massachusetts

for

Massachusetts Institute of Technology

Lincoln Laboratory

Approved for public release; distribution unlimited.

Scientific Report No. 13 (Vol. I)

MODIFIED DIPOLES:
I. THEORETICAL AND EXPERIMENTAL STUDY

Peter S. Kao

Prepared by

Harvard University

for

Massachusetts Institute of Technology

Lincoln Laboratory

under

Purchase Order No. C-782

Prime Contract No. F19628-70-C-0230

MODIFIED DIPOLES
I. THEORETICAL AND EXPERIMENTAL STUDY

By

Peter S. Kao

Division of Engineering and Applied Physics
Harvard University · Cambridge, Massachusetts

ABSTRACT

The 'modified dipole' has its origin in the consideration of the general properties of a satellite antenna which bears great resemblance to a dipole modified to incorporate at the center a conducting volume which is used to radiate electromagnetic waves and to house a power supply and radio frequency generators, etc. The object of this research is to pursue a theoretical and experimental exploration of the effects induced by the presence of the conducting volume on the antenna performance, i. e., input characteristics, current distribution along the surfaces of the entire radiating structure and radiation properties.

In Volume I a mathematical model consisting of a perfectly conducting sphere from which project the ends of a thin biconical antenna is chosen to simulate the actual sphere-centered thin dipole. The conical antenna is driven at its junction with the sphere by a rotationally symmetric electric field maintained across the gap by a biconical transmission line excited by the TEM mode. The attractive features of this model include the fact that it has surfaces that permit a simple specification of boundary conditions and, hence, a rigorous formulation for the electromagnetic fields and a shape such that its properties should come reasonably close to those of a modified cylindrical antenna as the cone angle becomes quite small.

The measurements of both input admittances and current distributions on modified dipoles (with either conical or cylindrical

antenna projecting from the sphere) are also presented in Volume I. Comparisons were also made between modified conical and cylindrical antennas with the same sphere radii and antenna heights. The radius of the cylindrical antenna is the same as the smaller end of the cone. The fact that the admittance curves for modified cylindrical and conical antennas involve only slight shifts suggests that by introducing an equivalent antenna length that is a little longer than the actual physical length of the conical antenna a good approximation is obtained for the cylindrical antenna.

An infinite set of algebraic equations was solved numerically in Volume II for small cone angles. Comparisons were made between the modified conical antenna and its limiting biconical antenna which provides both an extrapolatory numerical check for the modified conical antenna with shrinking central sphere and an understanding of the underlying physical phenomena. Theoretical and experimental results are in very good agreement.

Accepted for the Air Force
Joseph R. Waterman, Lt. Col. USAF
Chief, Lincoln Laboratory Project Office

A. THEORETICAL STUDY

1. INTRODUCTION

Great advances have been made in the fundamental understanding of the properties of a cylindrical antenna over a planar surface for the past decades [1]-[2], but relatively little has been known about the current distribution, input admittance and radiation pattern of a dipole antenna that is modified to incorporate a conducting volume at the center. Such an antenna has immediate practical application to spacecraft antennas, broadcasting antennas erected on a hilltop, self-contained field probes, etc. During the past years there has been considerable interest in obtaining information concerning the effects of central modification upon the behavior of a dipole. Some of the possible modified thin dipoles are shown in Fig. 1-1 in which a sphere-centered thin dipole seems attractive because it is mathematically tractable and still general enough to permit the estimation of the effect of the vehicle shape on the antenna performance by approximating the actual vehicle by the sphere. An earlier work by Papas and King [3] was done on the surface current distribution on a conducting sphere excited by a dipole along which a sinusoidal current is assumed. Later some experimental measurements of a monopole over a metal hemisphere on a ground plane were made by Iizuka [4] for $\beta_0 h = \pi/2$, π and 2π as a function of $\beta_0 b$(=.4-1.3). Tesche and Neureuther [5] have computed radiation patterns for two monopoles on a conducting sphere.

As shown in Fig. 1-2, an approximation has been made by replacing the cylindrical dipole by a thin biconical antenna which has great mathematical advantages in permitting the convenient specification of the boundary conditions and thus allowing a rigorous formulation. The earliest analysis of the biconical dipole was performed by Schelkunoff [6] who introduced the symmetric biconical antenna as a convenient model for studying the impedance properties of dipole antennas. In that paper is presented the limiting case of the thin symmetric biconical antenna. In later publications [7]-[8] he treated wider angle biconical antennas. Further work on symmetric biconical antennas was reported by Tai [9]-[10] and by Smith [11]. Papas and King [12] have calculated the input impedance of a

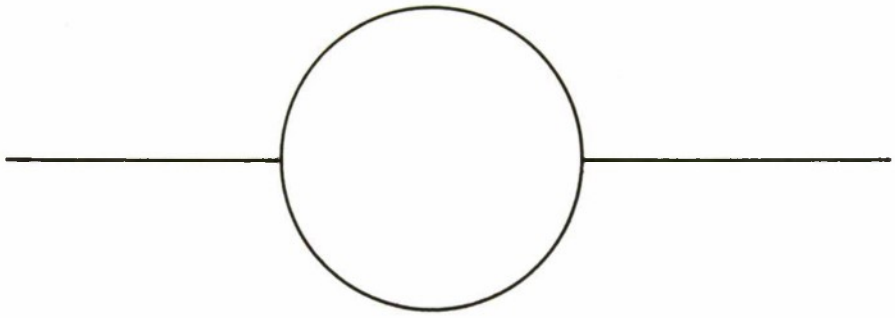

(a) SPHERE-CENTERED THIN DIPOLE

(b) CYLINDER-CENTERED THIN DIPOLE TYPE 1

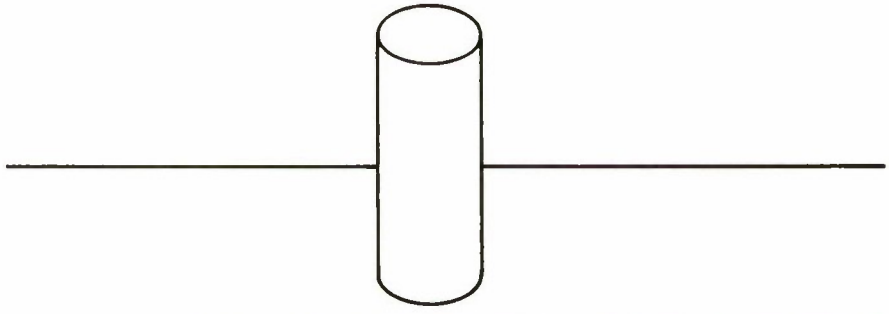

(c) CYLINDER-CENTERED THIN DIPOLE TYPE 2

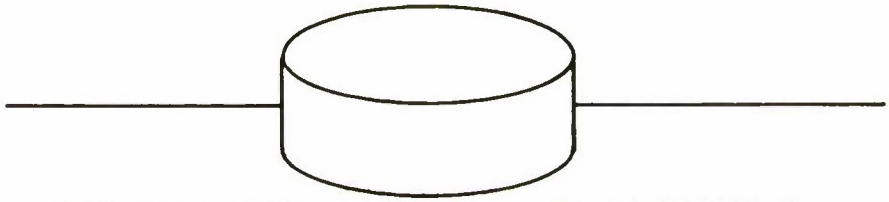

(d) PILLBOX-CENTERED THIN DIPOLE

FIG. 1-1 SOME MODIFIED THIN DIPOLES

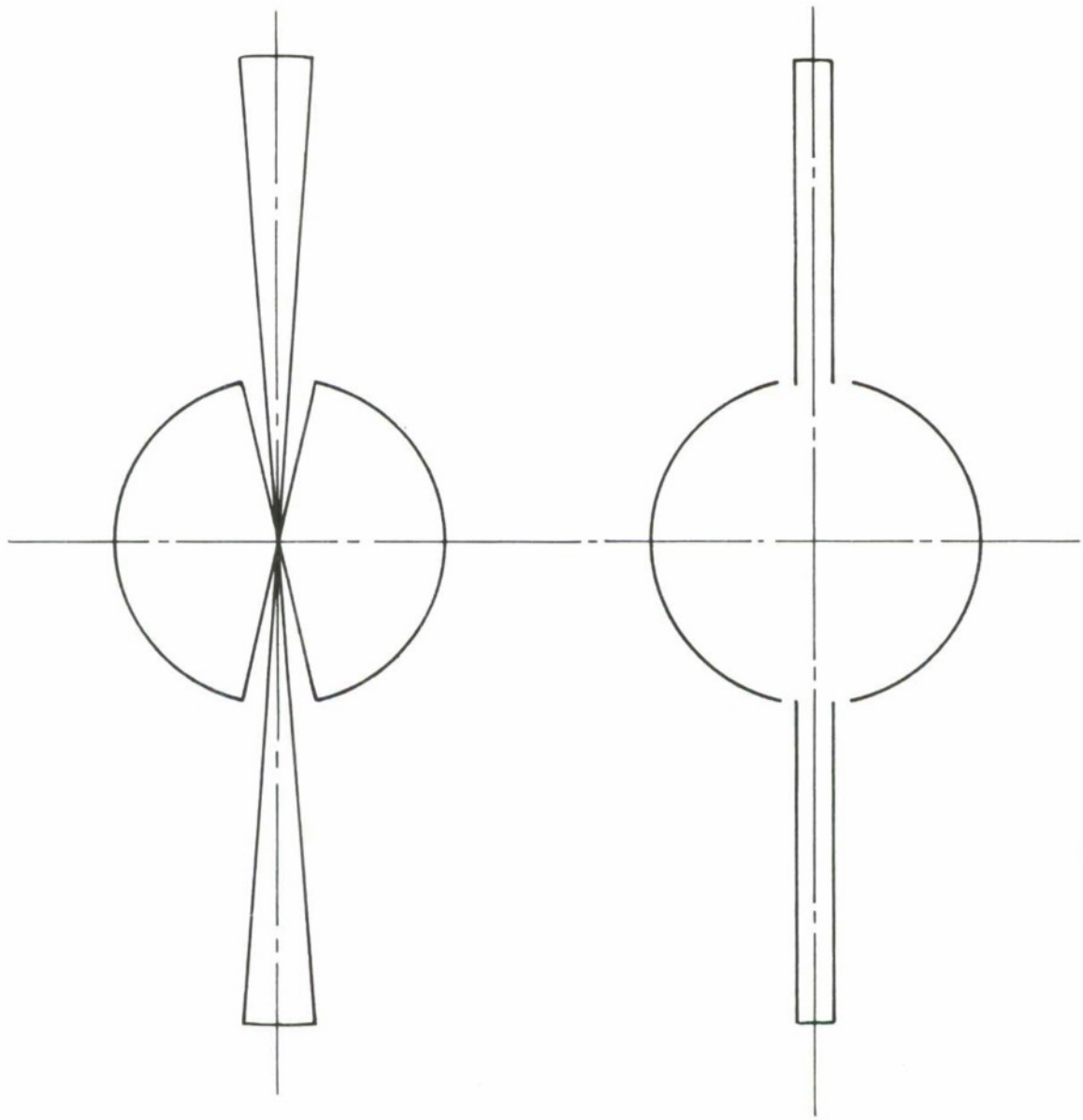

FIG. 1-2 (a) MODIFIED THIN CYLINDRICAL ANTENNA
(b) MODIFIED THIN CONICAL ANTENNA

wide-angle conical antenna fed by a coaxial line in which only the TEM mode in the antenna region and a series of modes in the radiation region were considered. Recently Bolle and Morganstern [13] obtained the input impedance and far-field pattern of a single conical antenna protruding from a sphere.

The present analysis consists of determining the distribution of current, the driving point admittance, and the radiation field. The study of this modified conical antenna can be made more revealing by constantly making comparisons with the corresponding limiting case of the biconical antenna which serves both as an extrapolatory check for the modified conical antenna and as a measure in selecting comparable sizes of cylindrical and conical antennas.

2. FORMULATION OF THE PROBLEM

(A) Equations for Spherical Waves with Rotational Symmetry

The first problem encountered in elucidating the radiation due to a spherical configuration (i.e., the boundary conditions of the radiating configuration are expressed conveniently in spherical coordinates R, θ, ϕ) is that of finding suitable representation for the field. This arises because the components of the intensity in spherical polar coordinates do not satisfy independent equations as do the Cartesian coordinates. Generally speaking, however, any electromagnetic field in a homogeneous isotropic medium in free space that is free from charges and currents can be expressed in terms of an electric Hertz vector and a magnetic Hertz vector both along a direction which can be chosen at will [14].

Thus, for a homogeneous region with dielectric constant ϵ and permeability μ, the electromagnetic field at points in space outside the radiating system is calculated from Hertz potentials using

$$E = -\nabla f + \beta^2 \pi_e - j\omega \nabla \times \pi_m \qquad (1\text{-}1)$$

and

$$B = -\nabla g + \beta^2 \pi_m + \frac{j\beta^2}{\omega} \nabla \times \pi_e \qquad (1\text{-}2)$$

where the time factor has been taken as $e^{j\omega t}$, $\beta = \omega \sqrt{\mu\epsilon}$ is the wave number

in the dielectric medium; ω is the angular frequency, f and g are arbitrary scalar functions and π_e and π_m are Hertz potentials of electric and magnetic type respectively. The part of the field computed from π_e is said to be of electric type and the part computed from π_m of magnetic type. Since π_e and π_m are mutually independent, fields of electric and magnetic type are independent.

The Hertzian potentials are defined in general to satisfy the following equations in free space:

$$\nabla \times \nabla \times \pi_e - \beta^2 \pi_e + \nabla f = 0 \tag{1-3}$$

$$\nabla \times \nabla \times \pi_m - \beta^2 \pi_m + \nabla g = 0 \tag{1-4}$$

By specializing the Hertzian potentials to point in radial direction (i. e. $\pi_e = \pi_{eR}\, R$ and $\pi_m = \pi_{mR}\, R$) and introducing the following definitions for f and g, namely

$$f = \frac{\partial \pi_{eR}}{\partial R} \tag{1-5a}$$

$$g = \frac{\partial \pi_{mR}}{\partial R} \tag{1-5b}$$

(1-3) and (1-4) are reduced to

$$\frac{\partial^2 \pi_R}{\partial R^2} + \nabla^2_{\theta,\Phi}\, \pi_R + \beta^2\, \pi_R = 0 \tag{1-6}$$

$$\pi_R = \pi_{eR} \text{ or } \pi_{mR}$$

where $\nabla^2_{\theta,\Phi}$ is that part of the Laplacian operator in spherical coordinates that involves differentiation only with respect to θ and Φ.

It should be noted that the above representation is only valid in general at points in free space. Thus the field due to an electric dipole not situated at the origin cannot be expressed in terms of π_{eR} and π_{mR} alone in any region which includes the dipole unless the dipole is directed along the radius vector. The same is true of the radial magnetic dipole.

For the case of interest at hand, it is convenient to assume complete rotational symmetry about the polar axis. Consequently, two

simplifications to equation (1-6) can be accomplished: first, all the terms involving differentiation with respect to Φ become zero; secondly, only the components of the field of electric type derived from the Hertzian potential π_{eR} are involved. Therefore, (1-6) reduces to

$$\frac{\partial^2 \pi_{eR}}{\partial R^2} + \frac{1}{R^2 \sin\theta} \frac{\partial}{\partial \theta} (\sin\theta \frac{\partial \pi_{eR}}{\partial \theta}) + \beta^2 \pi_{eR} = 0 \qquad (1-7)$$

and the non-vanishing field components in spherical coordinates are to be obtained from

$$E_R = \frac{\partial^2 \pi_{eR}}{\partial R^2} + \beta^2 \pi_{eR} \qquad (1-8)$$

$$E_\theta = \frac{1}{R} \frac{\partial^2 \pi_{eR}}{\partial \theta \partial R} \qquad (1-9)$$

$$B_\Phi = \frac{-j\beta^2}{\omega R} \frac{\partial \pi_{eR}}{\partial \theta} \qquad (1-10)$$

(B) Modified Conical Dipole

(1) Mathematical Model

As shown in Fig. 1-3, a modified conical dipole consists of two main parts: one of these consists of the two identical conducting cones DOD with half cone angle θ_0 and conducting cap DED that are segments of the boundary sphere of radius a; the other part is an inner conducting sphere of radius b concentric with the boundary sphere. The axis is along the polar axis of the spherical coordinates (R, θ, Φ) with the cone apex at the origin. The whole modified conical structure is rotationally symmetric about the polar axis and is immersed in air. It is center-driven by an idealized point generator at the apex of the cones with no internal impedance and an emf V_c^e. The protruding portion of the cones which extends from R = b to R = a functions as a dipole antenna while the remaining portion along with the inner sphere forms a biconical transmission line with angle θ_1, which supports mainly transverse

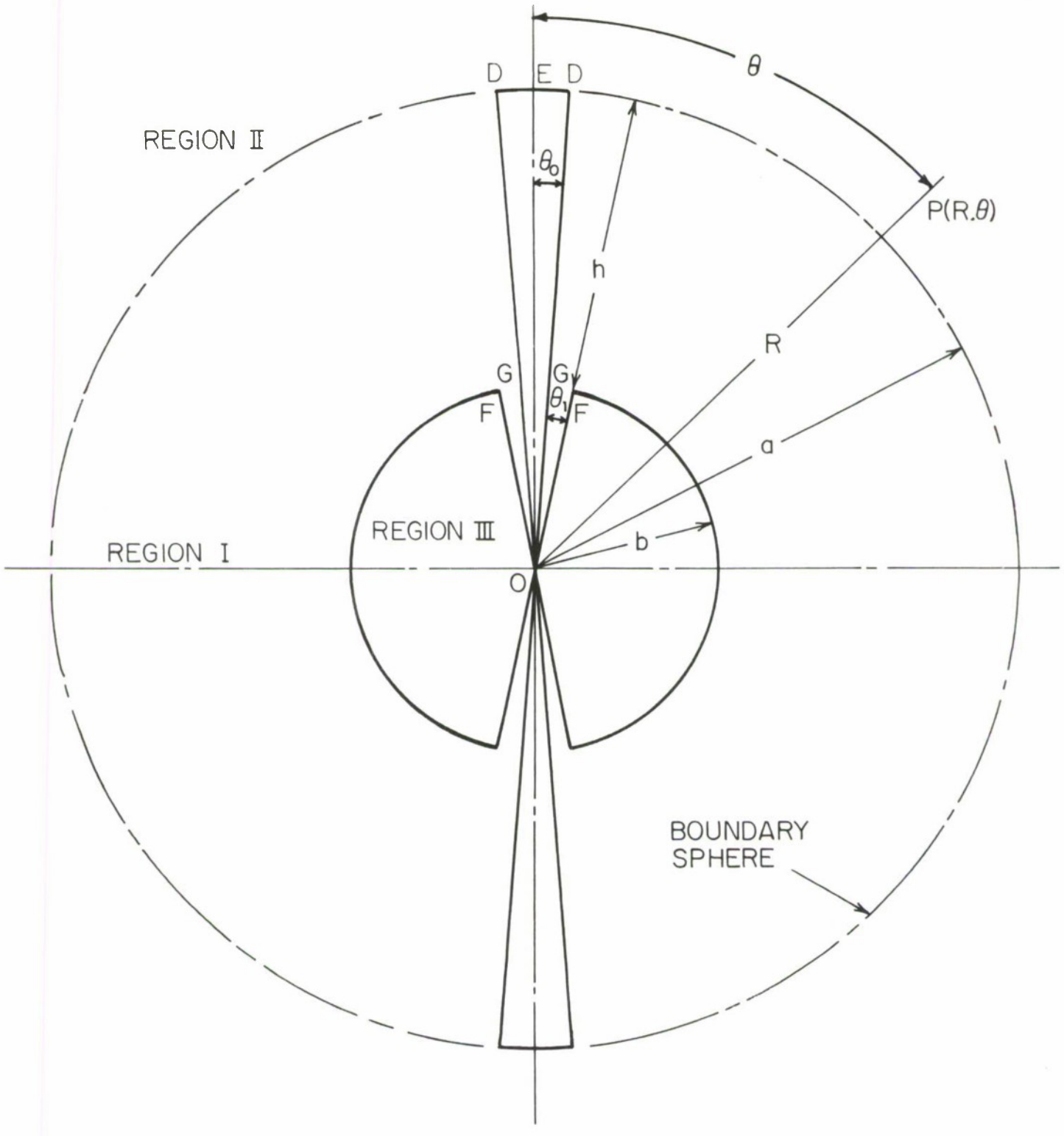

FIG. 1-3 MODIFIED THIN CONICAL ANTENNA

electromagnetic waves excited by the point generator at the origin. As a result, a finite radial E-field exists in the narrow band along the junctions between the cones and the sphere.

The basic properties to be studied are the distribution of the total current along the surfaces of both the conical dipole and the hemisphere and the input admittance characteristics of the dipole as seen at the terminal of the biconical transmission line. Hence for purposes of theoretical treatment, it is convenient to consider the antenna excitation as being applied across the gap at R = b. The gap width (i.e., $b \times \theta_1$) is assumed to be much smaller than the free space wave length. The driving voltage over the gap is defined as the line integral of the θ-component of the electric field along the meridian of the radius b, i.e.,

$$\int_{\theta_0}^{\pi-\theta_0} E_\theta b \, d\theta = V_0^e \tag{1-11}$$

For simplicity, the structure is assumed to be constructed of a perfectly conducting metal, the tangential component of the E field must disappear on the metallic surfaces, i.e.,

$$n \times E = 0 \tag{1-12}$$

is true on all conductors. Therefore, the specific boundary conditions on the conductors are

$$E_R = 0 \qquad \begin{matrix} \theta = \theta_0 \\ \theta = \pi - \theta_0 \end{matrix} \qquad \text{and} \quad b \leq R \leq a \tag{1-13a}$$

$$E_\theta = 0 \qquad \begin{matrix} \theta \leq \theta_0 \\ \theta \geq \pi - \theta_0 \end{matrix} \qquad \text{and} \quad R = a \tag{1-13b}$$

$$E_\theta = 0 \qquad \pi - \theta_0 - \theta_1 \geq \theta \geq \theta_0 + \theta_1 \quad \text{and } R = b \tag{1-13c}$$

$$E_\theta = \frac{V_0^e}{2b \cdot fn(\theta_0, \theta_1) \cdot \sin\theta} \qquad \begin{matrix} \theta_0 \leq \theta \leq \theta_0 + \theta_1 \\ \pi - \theta_0 - \theta_1 \leq \theta \leq \pi - \theta_0 \end{matrix} \qquad \text{and } R = b \tag{1-13d}$$

where

$$fn(\theta_0, \theta_1) = \ln(\cot \frac{\theta_0}{2}) - \ln(\cot \frac{\theta_0 + \theta_1}{2}) \qquad (1\text{-}13e)$$

In applying the boundary conditions (1-13a-d), it is convenient to treat the whole region in two parts (Fig. 1-3): an internal region I between the boundary sphere of radius a and inner sphere of radius b, and an external region II occupying all space where $R > a$. The conditions for the internal region are given by (1-13a, c, d); that for the external region by (1-13b). In addition, a condition of the field at infinity is necessary to ensure uniqueness. This condition is that the field behaves like outward traveling waves. In precise mathematical terms, these conditions are

$$|RE| < K \quad \text{and} \quad |RB| < K$$

$$R \cdot (\omega R \times B + \beta E) \quad 0 \qquad (1\text{-}14a)$$

$$R \cdot (\beta R \times E - \omega B) \quad 0 \qquad (1\text{-}14b)$$

uniformly with respect to direction as $R \to \infty$.

We note the boundary conditions (1-13a-d) are the same as those for the biconical antenna except for (1-13d) which accounts for the presence of the central sphere. One would expect that the complication introduced by satisfying the boundary conditions, (1-13c, d), would lead to the appearance of a large number of non-negligible complementary modes (TM modes) along with the TEM mode in the antenna region, and that these modes are important in the sense that they are closely connected with the current distribution. A $1/\sin\theta$ dependence of the θ-component of the electric field over the gap is employed to characterize the voltage maintained by the biconical transmission line. It is significant to note that for thin cones with a narrow driving gap, this assumption closely approximates the coaxial line which is used in the actual experimental set-up.

(2) Boundary Value Problem

The solution is formulated by considering two fundamental regions: the antenna region $b < R < a$, $\theta_0 \leq \theta \leq \pi - \theta_0$ and the radiation region

$R > a$, $0 \leq \theta \leq \pi$, in which the non-vanishing components of the fields, E_θ, E_R and B_Φ are expanded in series of functions appropriate to the two regions. The unknown constants in these series are determined by guaranteeing the continuity of B_Φ and E_θ across the boundary sphere at $R = b$, $\theta_0 \leq \theta \leq \pi - \theta_0$.

(i) General Solution of the Wave Equation

The solution of (1-7) is accomplished by the well-known method of separation of variables by setting

$$\pi_{eR} = T(\theta)S(R) \tag{1-15}$$

where T and S denote functions of θ and R respectively. The substitution of (1-15) in (1-7) and the division of both sides by T and S lead to the following equation:

$$-R^2 \left(\frac{1}{S} \frac{\partial^2 S}{\partial R^2} + \beta_0^2\right) = \frac{1}{T} \left[\frac{1}{\sin\theta} \frac{\partial}{\partial\theta} \left(\sin\theta \frac{\partial T}{\partial\theta}\right)\right] \tag{1-16}$$

Since the left-hand member of (1-16) is a function of R alone while the right-hand member is a function of θ alone, the two expressions can be equal only if both are equal to a constant. Let this be $\nu(\nu + 1)$, where ν is an arbitrary number. The resulting two ordinary differential equations are

$$\frac{d^2 S}{dR^2} + \left[\beta_0^2 - \frac{\nu(\nu+1)}{R^2}\right] S = 0 \tag{1-17}$$

$$\frac{1}{\sin\theta} \frac{d}{d\theta} \left(\sin\theta \frac{dT}{d\theta}\right) + \nu(\nu + 1)\, T = 0 \tag{1-18}$$

The radial equation (1-17) is Bessel's equation of order $\nu + 1/2$; its solutions are well-known and can be expressed in terms of general cylinder functions, namely,

$$S(\beta_0 R) = A_\nu J_{\nu+1/2}(\beta_0 R) + B_\nu N_{\nu+1/2}(\beta_0 R) \tag{1-19}$$

Alternatively, (1-19) can be expressed in terms of the so-called spherical Bessel functions as follows:

$$S(\beta_0 R) = \beta_0 R \left[a_\nu j_\nu(\beta_0 R) + b_\nu n_\nu(\beta_0 R)\right] \tag{1-20}$$

where

$$j_\nu(x) = \sqrt{\pi/2x}\, J_{\nu+1/2}(x) \tag{1-21a}$$

$$n_\nu(x) = \sqrt{\pi/2x}\, N_{\nu+1/2}(x) \tag{1-21b}$$

and A_ν, B_ν, a_ν and b_ν are arbitrary constants.

Equation (1-18) may be reduced to a more familiar form known as Legendre's equation by changing the independent variable from θ to $\mu = \cos\theta$. The transformed equation is

$$(1 - \mu^2) \frac{d^2T}{d\mu^2} - 2\mu \frac{dT}{d\mu} + \nu(\nu+1)\, T = 0 \tag{1-22}$$

A general solution of (1-22) is

$$T = c'_\nu P_\nu(\mu) + d'_\nu Q_\nu(\mu) \tag{1-23}$$

where $P_\nu(\mu)$ is a Legendre function of the first kind and $Q_\nu(\mu)$ a Legendre function of the second kind, both of order ν; c'_ν and d'_ν are arbitrary constants. When ν is not an integer, solutions of (1-22) may be written in the following form:

$$T = c_\nu P_\nu(\mu) + d_\nu P_\nu(-\mu) \tag{1-24}$$

It is to be noted that $P_\nu(\mu)$ is unity at $\theta = 0$, whereas $P_\nu(-\mu)$ is logarithmically infinite there.

So the general solution of the original equation (1-7) is a linear combination of the following form:

$$\pi_{eR} = \sum_\nu S_\nu(\beta_0 R)\, T_\nu(\theta) \tag{1-25a}$$

$$= \sum_\nu \beta_0 R \left[a_\nu j_\nu(\beta_0 R) + b_\nu n_\nu(\beta_0 R)\right] \left[c'_\nu P_\nu(\mu) + d'_\nu Q_\nu(\mu)\right] \tag{1-25b}$$

$$= \sum_\nu \beta_0 R \left[a_\nu j_\nu(\beta_0 R) + b_\nu n_\nu(\beta_0 R)\right] \left[c_\nu P_\nu(\mu) + d_\nu P_\nu(-\mu)\right] \tag{1-25c}$$

(ii) Antenna Region I

The entire field in the antenna region is the sum of the fields for the dominant mode (i.e., $v = 0$) and the complementary modes ($v \neq 0$). Since $\vartheta = 0$ and the origin is not included in the antenna region, both Legendre functions and spherical Bessel functions of the second kind have no singularities.

To construct the appropriate form of the solution in the antenna region $b \leq R \leq a$, it is convenient to separate the purely transverse electromagnetic (TEM) waves from the transverse magnetic waves (TM) in general. The former case has some useful analogies with transmission-line theory. For $v = 0$,

$$(\pi^{I}_{eR})_{v=0} = [C_0 + B_0 \ln(\cot\tfrac{\theta}{2})] \cdot (a_0 \sin\beta_0 R_b - b_0 \cos\beta_0 R_b) \qquad (1\text{-}26)$$

where $R_b = R - b$. Hence the non-vanishing components are

$$(E_\vartheta)_{v=0} = \frac{\xi_0}{2\pi R \sin\theta} (a'_0 \cos\beta_0 R_b + b'_v \sin\beta_0 R_b) \qquad (1\text{-}27a)$$

$$(B_\varphi)_{v=0} = \frac{-j}{2\pi \nu_0 R \sin\theta} (a'_0 \sin\beta_0 R_b - b'_0 \cos\beta_0 R_b) \qquad (1\text{-}27b)$$

where ξ_0 is the characteristic impedance of free space (i.e., 120π ohms) and ν_0 the reluctivity of space (i.e., $\frac{1}{4\pi} \times 10^7$ meter/henry). The expressions for E_θ and B_φ in (1-27a, b) may be interpreted as representing standing spherical waves while treating the protruding bi-conical structure as a terminated transmission line.

The boundary condition that must be satisfied in region I is given by (1-13c), i.e., $E_R = 0$ at $\vartheta = \theta_0$ and $\pi - \theta_0$ for $b \leq R \leq a$, together with the property of anti-symmetry of E_R with respect to the equatorial plane ($\theta = \pi/2$ - plane), i.e., $E^I_R(\theta) = -E^I_R(\pi - \theta)$. These conditions lead to the following equations:

$$T_v(\theta) = 2c_v L_v(\theta) \qquad (1\text{-}28)$$

where

$$L_v(\theta) = \frac{1}{2}[P_v(\cos\theta) - P_v(-\cos\theta)] \qquad (1\text{-}29)$$

which satisfies the Legendre equation (1-22).

For a given half cone angle θ_0, therefore, there is an infinite set of characteristic values designated by v. These values must be determined from the characteristic equation, i.e.,

$$L_v(\theta_0) = L_v(\pi - \theta_0) = 0 \tag{1-30}$$

The fact that the use of (1-24) instead of (1-23) eliminates at the outset the possibility that v may be an integer may seem to be a severe limitation. Actually this is not the case at least for the application to the thin conical antenna for which the present analysis is intended. That this is true can easily be seen by applying the same set of boundary conditions to (1-23) and assuming that there is an integral $v=n$. Then the anti-symmetric property of E_R requires that $P_n(\mu)$ and $Q_n(\mu)$ cannot both be used due to the fact that $P_n(-\mu) = (-1)^n P_n(\mu)$ and $Q_n(-\mu) = (-1)^{n+1} Q_n(\mu)$. Then the vanishing of E_R along the conical surfaces leads to either $P_n(\mu_0) = 0$ for n even or $Q_n(\mu_0) = 0$ for n odd. For the small cone angle $\theta_0 \leq 4^o$, the first possible values of n for $P_n(\mu_0) = 0$ are approximately equal to x_0/θ_0 (not necessarily an integer) where $x_0 = 2.405$ is the first root of Bessel function $J_0(x_0) = 0$. Therefore unles $\theta_0 = 2.405 \times 10^{-2}$ radians ($n=100$) the possible first integer is far greater than 100; while for $Q_n(\mu_0) = 0$, the possible solution for n is $\psi(n+1) = -\gamma - \ln(\sin \frac{\theta_0}{2})$ which, again, is satisfied only at a special angle. Therefore, the use of (1-23) is actually quite general enough to cover the range of interest.

Accordingly, the non-vanishing complementary components of the electromagnetic fields in region I are obtained from (1-25c), with (1-8)-(1-10) and (1-30). They are

$$(E_\theta^I)_{v\neq 0} = \frac{2\beta_0}{R} \sum_v R'_v(\beta_0 R) L'_v(\theta) \tag{1-31a}$$

$$(E_R^I)_{v\neq 0} = \frac{2}{R^2} \sum_v v(v+1) R_v(\beta_0 R) L_v(\theta) \tag{1-31b}$$

$$(B_\phi^I)_{v\neq 0} = \frac{-2j\beta_0^2}{\omega R} \sum_v R_v(\beta_0 R) L'_v(\theta) \tag{1-31c}$$

where primes on R_ν and L_ν denote differentiation with respect to the arguments, and

$$R_\nu(\beta_0 R) = a'_\nu J'_\nu(\beta_0 R) + b'_\nu N'_\nu(\beta_0 R) \tag{1-32a}$$

$$J_\nu(x) = x\, j_\nu(x) \tag{1-32b}$$

$$N_\nu(x) = x\, n_\nu(x) \tag{1-32c}$$

the arbitrary constants $a'_\nu = c'_\nu a_\nu$ and $b'_\nu = c'_\nu b_\nu$. The summation signs in (1-31a-c) indicate that contributions from all the roots of $L_\nu(\mu_0) = 0$ must be included in the formulation.

To satisfy another boundary condition (1-13d), let

$$E^I_\theta\big|_{R=b} = \frac{a'_0 \xi_0}{2\pi b \sin\theta} + \frac{2\beta_0}{b} \sum_\nu R'_\nu(\beta_0 b) L_\nu(\theta)$$

$$= \frac{V^e_0}{2b}\, g(\theta, \theta_0) \tag{1-34}$$

where $g(\theta, \theta_0)$ is a function describing the driving condition of the system and

$$g(\theta, \theta_0) = \frac{1}{fn(\theta_0, \vartheta_1)\sin\theta} \left[\mathrm{sgn}(\theta-\theta_0) - \mathrm{sgn}(\theta-\theta_0-\theta_1) + \mathrm{sgn}(\theta+\theta_0+\theta_1-\pi) - \mathrm{sgn}(\theta+\theta_0-\pi)\right] \tag{1-35}$$

where sgn(x) denotes the Heaviside unit function equal to 1 if $x > 0$ and zero if $x < 0$.

It is well known from the theory of Legendre functions and the characteristic equation, i.e., $L_\nu(\theta_0) = 0$, that the set of functions $1/\sin\theta$, $L'_\nu(\theta)$ form a set of orthogonal functions in the region $\theta_0 \le \theta \le \pi - \theta_0$ in association with a weighting function $\sin\theta$, namely

$$\int_{\theta_0}^{\pi-\theta_0} L'_s(\theta)\, L'_t(\theta) \sin\theta\, d\theta = \delta_{st} \tag{1-36}$$

where δ_{st} is the Kronecker delta:

$$\delta_{st} = \begin{cases} 1 & \text{if } s=t \\ 0 & \text{if } s\neq t \end{cases}$$

and s and t are the roots of the characteristic equation $L_v(\theta_0) = 0$.

In order to determine the constant a'_0 and the relation between a'_v and b'_v from (1-34), first integrate (1-34) with respect to θ from $\theta = \theta_0$ to $\theta = \pi-\theta_0$. Since from (1-30), the second term in (1-34) integrates to zero, it follows that

$$a'_0 = \frac{\pi V_0^e}{\xi_0 \ln(\cot\frac{\theta_0}{2})} = \frac{V_0^e}{Z_c} \tag{1-37}$$

where $Z_c = 120 \ln(\cot\frac{\theta_0}{2})$ is the characteristic impednace of the conical antenna.

Equation (1-37) shows that the constant a'_0 is determined uniquely if the driving voltage and conical angle are specified.

Since the determination of the relations for a'_v and b'_v involve the driving condition, it is convenient to begin with the multiplication of (1-34) by $L'_v(\theta)\sin\theta\, d\theta$ and continue the integration with respect to θ from $\theta=\theta_0$ to $\theta=\pi-\theta_0$. With the orthogonal properties of $L'_v(\theta)$ in (1-36), it follows directly that

$$a'_v = \alpha_v - \eta_v b'_v \tag{1-38}$$

where

$$\alpha_v = \frac{V_0^e L_v(\theta_0+\theta_1)}{2\beta_0 J_{vv} J'_v(\beta_0 b)\, fn(\theta_0,\theta_1)\, v(v+1)} \tag{1-39a}$$

$$\eta_v = \frac{N'_v(\beta_0 b)}{J'_v(\beta_0 b)} \tag{1-39b}$$

and

$$J_{vv} = \int_{\theta_0}^{-\theta_0} [L'_v(\theta)]^2 \sin\theta \, d\theta$$

$$= \frac{2(1-\mu_0^2)}{(2v+1)} \left[\frac{\partial L_v(\mu)}{\partial v} \quad \frac{\partial L_v(\mu)}{\partial \mu}\right]\Big|_{\mu=\mu_0} \tag{1-39c}$$

Therefore, the non-vanishing components of the electromagnetic fields can be rearranged as follows:

$$E^I_\theta = \frac{\xi_0}{2\pi R \sin\theta} (a'_0 \cos\beta_0 R_b + b'_0 \sin\beta_0 R_b)$$

$$+ \frac{2\beta_0}{R} \sum_v [a_v J'_v(\beta_0 R) + b'_v M_v(\beta_0 R)] L'_v(\theta) \tag{1-40a}$$

$$E^I_R = \frac{2}{R^2} \sum_v v(v+1)[a_v J_v(\beta_0 R) + b'_v M_v(\beta_0 R)] L_v(\theta) \tag{1-40b}$$

$$B^I_\phi = \frac{j}{2\pi \nu_0 R \sin\theta} (a'_0 \sin\beta_0 R_b - b'_0 \cos\beta_0 R_b)$$

$$- \frac{j2\beta_0^2}{\omega R} \sum_v [a_v J_v(\beta_0 R) + b'_v M_v(\beta_0 R)] L'_v(\theta) \tag{1-40c}$$

where

$$M_v(x) = N_v(x) - \eta_v J_v(x) \tag{1-41}$$

(iii) Radiation Region II

In the region external to the antenna (i. e., $R > a$), the fields are also of the TM type. However, the angular functions must be periodic and finite for all values of θ from $\theta=0$ to $\theta=\pi$. So the appropriate expression for the Hertzian potential in the radiation region II is given by

$$\pi_{eR}^{II} = \sum_k{}' \; c_k R_k(\beta_0 R) P_k(\theta) \tag{1-42}$$

where

$$R_k(x) = x\, h_k^{(2)}(x) \tag{1-43}$$

and the prime on the sign of summation denotes that the sum is over odd values of k, i.e., $\sum_k{}' = \sum_{k=1,3,5\cdots}$. The even values of k are excluded due to the fact that the radial electric field is odd in μ; further, the radial function R_k, which is a solution of (1-17), has the required property that $R_k \to \exp(-j\beta_0 R)$ for $R \to \infty$.

So the non-vanishing components of the electromagnetic field are obtained from (1-8)-(1-10); they are

$$E_\theta^{II} = \frac{-j\xi_0}{2\pi R} \sum_k{}' \frac{b_k}{k(k+1)} \frac{R_k'(\beta_0 R)}{R_k(\beta_0 a)} P_k'(\theta) \tag{1-44a}$$

$$E_R^{II} = \frac{-j}{2\pi\omega\epsilon_0 R^2} \sum_k{}' b_k \frac{R_k(\beta_0 R)}{R_k(\beta_0 a)} P_k(\theta) \tag{1-44b}$$

$$B_\Phi^{II} = \frac{-1}{2\pi\nu_0 R} \sum_k{}' \frac{b_k}{k(k+1)} \frac{R_k(\beta_0 R)}{R_k(\beta_0 a)} P_k'(\theta) \tag{1-44c}$$

The primes on R_k and P_k denote differentiation with respect to the argument. We have to note that there is no TEM mode in the region II.

It remains to impose conditions at the inner boundary of region II so that the tangential electric field vanishes on the spherical caps of the antenna and the entire electromagnetic field is continuous across the rest of the mathematical boundary sphere. The conditions are

$$E_\theta^{II} = 0 \qquad \begin{matrix} 0 \le \theta \le \theta_0 \\ \pi - \theta_0 \le \theta \le \pi \end{matrix} \qquad \text{at} \quad R = a \tag{1-45}$$

$$\begin{aligned} E_\theta^{II} &= E_\theta^{I} \\ B_\Phi^{II} &= B_\Phi^{I} \end{aligned} \qquad \theta_0 \le \theta \le \pi - \theta_0 \quad \text{at} \quad R = a \tag{1-46}$$

Since the continuity of tangential magnetic field B_Φ implies the continuity of E_R, it follows that it is sufficient to impose at boundary the continuity of E_θ and B_Φ.

The substitution of (1-44) in (1-45) gives

$$\sum_k{}' \frac{b_k}{k(k+1)} P'_k(\theta)\, \rho_k(\beta_0 a) = 0 \qquad (0 \leq \theta \leq \theta_0,\ \pi - \theta_0 \leq \theta \leq \pi) \tag{1-47}$$

where

$$\rho_k(x) = \frac{R'_k(x)}{R_k(x)} \tag{1-48}$$

Similarly the substitution of (1-40a) and (1-44a) in (1-46) gives

$$\sum_k{}' \frac{b_k \mu_k(\beta_0 a)}{k(k+1)} P'_k(\theta) = \frac{j}{\sin\theta}(a'_0 \cos\beta_0 h + b'_0 \sin\beta_0 h) + j4\pi\omega\epsilon_0 \sum_v [a_v J'_v(\beta_0 a) + b'_v M'_v(\beta_0 a)] L'_v(\theta) \qquad (\theta_0 \leq \theta \leq \pi - \theta_0,\ R = a) \tag{1-49}$$

where $h=a-b$ denotes the antenna height.

Finally substitution of (1-40c) and (1-44c) into (1-46) gives

$$\sum_k{}' \frac{b_k}{k(k+1)} P'_k(\theta) = \frac{j}{\sin\theta}(a'_0 \sin\beta_0 h - b'_0 \cos\beta_0 h) + j4\pi\omega\epsilon_0 \sum_v [a_v J_v(\beta_0 a) + b'_v M_v(\beta_0 a)] L'_v(\theta) \qquad (\theta_0 \leq \theta \leq \pi - \theta_0,\ R = a) \tag{1-50}$$

The above system of equations involves two independent sets of orthogonal functions whose ranges of orthogonality are different for the two regions, i.e., $R < a$ and $R > a$.

Some important properties of integrals involving products of Legendre functions are listed in Appendix A. Solutions for (1-47), (1-49) and (1-50) can be carried out by first integrating (1-50) with respect to θ from $\theta = \theta_0$ to $\pi - \theta_0$. This gives

$$b'_0 = a'_0 \tan\beta_0 h - \frac{j}{\cos\beta_0 h \ln(\cot\frac{\theta_0}{2})} \sum_k{}' \frac{b_k}{k(k+1)} P_k(\theta_0) \tag{1-51}$$

The determination of constant b'_v begins with the multiplication of (1-50) by $L'_v(\theta)\sin\theta\, d\theta$ and the integration with respect to θ from $\theta = \theta_0$ to $\pi - \theta_0$. It follows directly that

$$b'_\nu = \frac{-j}{4\pi\omega\epsilon_0 \nu(\nu+1)\, M_\nu(\beta_0 a) J_{\nu\nu}} \sum_k{}' b_k J_{\nu k} - a_\nu \frac{J_\nu(\beta_0 a)}{M_\nu(\beta_0 a)} \qquad (1\text{-}52)$$

An additional relation between b'_ν and b_k is obtained from (1-47) and (1-49) by first multiplying by $\frac{\partial P_r(\theta)}{\partial \theta} \sin\theta \, d\theta$ and then integrating with respect to θ from $\theta = 0$ to π. This gives

$$\frac{2b_r}{2r+1} \rho_r(\beta_0 a) = -2j(a'_0 \cos\beta_0 h + b'_0 \sin\beta_0 h) P_r(\theta_0) + j4\pi\omega\epsilon_0 \sum_\nu [a_\nu J'_\nu(\beta_0 a) + b'_\nu M'_\nu(\beta_0 a)] r(r+1) J_{\nu r} \qquad (1\text{-}53)$$

or, after rearrangement and substitution of (1-37), (1-39a) and (1-52) into (1-53), one obtains

$$\frac{2\rho_r(\beta_0 a)}{2r+1} b_r + \frac{2\tan\beta_0 h\, P_r(\theta_0)}{\ln(\cot\frac{\theta_0}{2})} \sum_k{}' \frac{P_k(\theta_0)}{k(k+1)} b_k - r(r+1) \sum_\nu \sum_k{}' \frac{J_{\nu r} J_{\nu k}}{\nu(\nu+1) J_{\nu\nu}} \frac{M'_\nu(\beta_0 a)}{M_\nu(\beta_0 a)} b_k = \frac{-2jV_0^e}{Z_c \cos\beta_0 h} P_r(\theta) + j4\pi\omega\epsilon_0 r(r+1) \sum_\nu{}' a_\nu J_{\nu r} \left[J'_\nu(\beta_0 a) - \frac{J_\nu(\beta_0 a) M'_\nu(\beta_0 a)}{M_\nu(\beta_0 a)}\right] \qquad (1\text{-}54)$$

Note that in (1-52) and (1-53) r had only those values assumed by k in the sum $\sum_k{}'$, i.e., r is odd in (1-54).

Further simplication of (1-54) can be accomplished by means of the fact that

$$\frac{J_{\nu r} J_{\nu k}}{J_{\nu\nu}} \quad \frac{-2(2\nu+1)(1-\mu_0^2) P_k(\theta_0) P_r(\theta_0)}{[k(k+1) - \nu(\nu+1)][r(r+1) - \nu(\nu+1)]} \frac{d\nu}{d\mu_0} \qquad (1\text{-}55)$$

and the Wronskian

$$M_v J'_v - M'_v J_v = -1 \tag{1-56}$$

With substitution of (1-55) and (1-56) into (1-54) and some rearrangement of the formulation, we obtain the following infinite set of linear equations:

$$\sum'_k C_{rk} b_k = -D_r = -D_{r1} - D_{r2} \tag{1-57}$$

$$r = 1, 3, 5 \ldots$$

where

$$D_{r1} = \frac{2jV_0^e P_r(\theta_0)}{r(r+1) Z_c \cos\beta_0 h} \tag{1-58a}$$

$$D_{r2} = \frac{-j V_0^e}{60} P_r(\theta_0) \sum'_v C_v \frac{2v+1}{v(v+1)} \frac{(1-\mu_0^2) \frac{\partial v}{\partial \mu_0}}{[r(r+1) - v(v+1)] A_v} \tag{1-58b}$$

$$C_v = \frac{L_v(\theta_0 + \theta_1)}{(1-\mu_0^2) fn(\theta_0, \theta_1) L'_v(\mu_0)} \tag{1-58c}$$

$$A_v = M_v(\beta_0 a) J'_v(\beta_0 b) \tag{1-58d}$$

and

$$C_{rk} = V_{rk} + E_{rk} - \delta_{rk} B_k \tag{1-58e}$$

$$V_{rk} = \frac{-240 \tan\beta_0 h P_r(\theta_0) P_k(\theta_0)}{Z_c k(k+1) r(r+1)} \tag{1-58f}$$

$$E_{rk} = -2(1-\mu_0^2) P_r(\theta_0) P_k(\theta_0)$$

$$\sum'_v \frac{2v+1}{v(v+1)} \frac{M'_v(\beta_0 a)}{M_v(\beta_0 a)} \frac{\frac{\partial v}{\partial \mu_0}}{[k(k+1)-v(v+1)][r(r+1)-v(v+1)]} \tag{1-58g}$$

$$B_k = \frac{2\rho_r(\beta_0 a)}{(2r+1)\, r\,(r+1)} \qquad (1\text{-}58h)$$

Since r and k can only assume odd integral values, the subscripts used in (1-57) do not indicate the actual position of the elements in the coefficient matrix, but rather C_{rk} denotes the element in the $(r+1)/2$ row and $(k+1)/2$ column in the corresponding coefficient matrix. The same is true for the column vectors b_k and D_r. Hence, a 3 x 3 matrix looks as follows:

$$\begin{bmatrix} C_{11} & C_{13} & C_{15} \\ C_{31} & C_{33} & C_{35} \\ C_{51} & C_{53} & C_{55} \end{bmatrix} \cdot \begin{bmatrix} b_1 \\ b_3 \\ b_5 \end{bmatrix} = - \begin{bmatrix} D_1 \\ D_3 \\ D_5 \end{bmatrix}$$

D_{r1} and D_{r2} on the right-hand side of (1-57) can be interpreted as the source functions for generating the coefficients b_k's, while D_{r1} is related to the conical antenna and D_{r2} is mainly associated with the presence of the inner conducting sphere. The effect of the inner conducting sphere is readily measured by the magnitude of D_{r2} relative to D_{r1}.

The infinite set of linear equations (1-57) is formulated on a general basis with no restrictions on the cone angle θ_0, the sphere radius b and antenna length h. However, (1-57) has a singular term when the antenna height approaches $\lambda/4$, $3\lambda/4 \cdots$, namely

$$V_{rk} \approx \tan\beta_0 h \to \infty \quad \text{and} \quad D_{r1} \approx \sec\beta_0 h \to \infty$$

$$(\beta_0 h = \pi/2,\ 3\pi/2 \cdots)$$

The singularity can be removed by multiplying both sides of (1-57) by $\cos\beta_0 h$ and then letting h approach a quarter wave length. This gives

$$\sum_k{}' \frac{P_k(\theta_0)}{k(k+1)}\, b_k = \frac{-jV_0^e}{120} \qquad (1\text{-}59)$$

Equation (1-59) is actually nothing more than (1-51) which expresses the constant b'_0 in terms of a'_0 and a linear combination of the b_k's. The procedures which lead to the expression for b'_0 in (1-51) were not valid since both sides were divided by a quantity which vanished at the particular antenna lengths.

To find an appropriate formulation for the solutions at the above particular antenna lengths, it is necessary to look back at the more fundamental equations i. e., (1-47), (1-49), and (1-50) and take different procedures in deriving an infinite set of linear equations.

Solutions for (1-47), (1-49), and (1-50) can now be obtained by first integrating (1-47) with respect to θ from $\theta = \theta_0$ to $\theta = \pi - \theta_0$. This gives

$$b'_0 = - a'_0 \cot \beta_0 h - \frac{j}{\ln(\cot \frac{\theta_0}{2}) \sin \beta_0 h} \sum_k{}' \frac{b_k \rho_k(\beta_0 a)}{k(k+1)} P_k(\theta_0) \tag{1-60}$$

The determination of the constant b'_v begins with the multiplication of (1-49) by $L'_v(\theta) \sin\theta \, d\theta$ and continues with the integration with respect to θ from $\theta = \theta_0$ to $\pi - \theta_0$. It follows that

$$b'_v = \frac{-j}{4\pi\omega\epsilon_0} \frac{1}{v(v+1) M'_v(\beta_0 a) J_{vv}} \sum_k{}' b_k \rho_k(\beta_0 a) J_{vk} - a_v \frac{J'_v(\beta_0 a)}{M'_v(\beta_0 a)} \tag{1-61}$$

An additional relation between b'_v and b_k is obtained from (1-47) and (1-50) by first multiplying by $\frac{\partial P_r(\theta)}{\partial \theta} \sin\theta \, d\theta$ and then integrating with respect to θ from $\theta = 0$ to $\theta = \pi$. This gives

$$\begin{aligned} \frac{2b_r}{2r+1} = & - \sum_k{}' \frac{b_k}{k(k+1)} [\rho_k(\beta_0 a) - 1] Q_{rk} \\ & - 2j(a'_0 \sin\beta_0 h - b'_0 \cos\beta_0 h) P_r(\theta_0) \\ & + j4\pi\omega\epsilon_0 \sum_v{}' [a_v J_v(\beta_0 a) + b'_v M_v(\beta_0 a)] r(r+1) J_{vr} \end{aligned} \tag{1-62}$$

where

$$Q_{rk} = Q_{kr} = \left(\int_0^{\theta_0} + \int_{\pi-\theta_0}^{\pi} \right) P'_k(\theta)\, P'_r(\theta)\, \sin\theta\, d\theta \qquad (1\text{-}63)$$

Rearrangement and the substitution of (1-60), (1-61), (1-37a), (1-55) and (1-56) into (1-62) gives

$$\sum_k{}' C'_{rk}\, b_k = - D'_r = - D'_{r1} - D'_{r2} \qquad (1\text{-}64)$$

where

$$D'_{r1} = \frac{2jV_0^e P_r(\theta_0)}{Z_c \sin\beta_0 h \cdot r(r+1)} \qquad (1\text{-}65a)$$

$$D'_{r2} = \frac{j V_0^e}{60} P_r(\theta_0)(1-\mu_0^2) \sum_v \frac{C_v}{A'_v} \frac{\frac{\partial v}{\partial \mu_0}}{[r(r+1) - v(v+1)]} \qquad (1\text{-}65b)$$

and

$$A'_v = M'_v(\beta_0 a)\, J'_v(\beta_0 b) \qquad (1\text{-}65c)$$

$$C'_{rk} = D'_{rk} + V'_{rk} + E'_{rk} - \delta_{rk} B'_{rk} \qquad (1\text{-}65d)$$

$$D'_{rk} = \frac{[1 - \rho_k(\beta_0 a)]\, Q_{rk}}{r(r+1)\, k(k+1)} \qquad (1\text{-}65e)$$

$$V'_{rk} = \frac{-240 \cot\beta_0 h\, \rho_k(\beta_0 a)\, P_k(\theta_0)\, P_r(\theta_0)}{Z_c\, k(k+1)\, r(r+1)} \qquad (1\text{-}65f)$$

$$E'_{rk} = -2(1-\mu_0^2)\, \rho_k(\beta_0 a)\, P_r(\theta_0)\, P_k(\theta_0) \sum_v \frac{2v+1}{v(v+1)} \frac{M_v(\beta_0 a)}{M'_v(\beta_0 a)} \frac{\frac{\partial v}{\partial \mu_0}}{[k(k+1) - v(v+1)][r(r+1) - v(v+1)]} \qquad (1\text{-}65g)$$

$$B'_{rk} = \frac{2}{(2r+1)\cdot r(r+1)} \tag{1-65h}$$

It is convenient to denote (1-57) as the first set of linear equations in which the antenna lengths $\beta_0 h = \pi/2,\ 3\pi/2,\ \ldots$ are excluded, and (1-62) as the second set of linear equations in which $\beta_0 h = \pi,\ 2\pi,\ \ldots$ are excluded. The combination of the first and second sets of linear equations adequately covers the whole range of antenna lengths.

Note that the driving terms in both the first set (i.e., $-D_r$) and second set (i.e., $-D'_r$) are linearly proportional to the driving voltage V_0^e across the gap. Hence, the solutions for both sets of linear equations (i.e., b_k's) are also in linear proportion to V_0^e. As a result of the linearity of Maxwell's equations, all the field quantities must also be in direct proportion to the values of V_0^e.

(iv) Electromagnetic Fields in Antenna Region

The electromagnetic fields (i.e., E_θ, E_R, B_Φ) in the antenna region I are of special interest in the present analysis, since all of the important characteristics of the modified dipole, i.e., the current distributions and the input admittances, depend largely upon how accurately these fields are calculated. These fields are related to the current and charge distributions over the surfaces of the antenna by the following boundary conditions;

$$n \times B = -I_d/\nu_0 \tag{1-66}$$

and

$$n \cdot E = -\eta_d/\epsilon_0 \tag{1-67}$$

where η_d is the surface density of free charge and I_d the surface density of conduction current. The current at the driving point determines the input admittance. All the fields inside region I can be expressed in terms of linear combination of the b_k's, which are the solutions of the infinite set of linear equations (1-57) and (1-64).

To find explicit expressions for the B_Φ in terms of the b_k's, the first set of linear equations will be examined first. The substitution of

(1-37), (1-39a), (1-51) and (1-52) into (1-40c) with the aid of the formulae in the appendices leads to (1-68) below. Note, however, that the b_k's are linearly related to V_0^e so no generality is lost by replacing b_k by $b_k V_0^e$ where b_k denotes the solution for $V_0^e = 1$. Thus,

$$(B_\Phi^I)_1(\theta, R) = (B_\Phi^I)_{1D} + (B_\Phi^I)_{1C} + (B_\Phi^I)_{1E} \tag{1-68}$$

where the subscript 1 denotes the first set of linear equations, and

$$(B_\Phi^I)_{1D} = \frac{V_0^e}{2\pi \nu_0 Z_c R \sin\theta} \left[-j(\sin\beta_0 R_b - \cos\beta_0 R_b \tan\beta_0 h)\right.$$

$$\left. + \frac{120 \cos\beta_0 R_b}{\cos\beta_0 h} \sum_k{}' \frac{b_k}{k(k+1)} P_k(\theta_0)\right] \tag{1-69a}$$

$$(B_\Phi^I)_{1C} = \frac{-\sin\theta\ V_0^e}{2\pi \nu_0 R} \sum_k{}' \sum_v \frac{2v+1}{v(v+1)} \frac{P_k(\theta_0)}{[k(k+1) - v(v+1)]} \cdot$$

$$\frac{L_v'(\mu)}{L_v'(\mu_0)} \frac{M_v(\beta_0 R)}{M_v(\beta_0 a)} \frac{\partial v}{\partial \mu_0} b_k \tag{1-69b}$$

$$(B_\Phi^I)_{1E} = \frac{-j\beta_0 \sin\theta}{2\omega R(1-\mu_0^2)} \frac{V_0^e}{fn(\theta_0, \vartheta_1)} \sum_v \frac{2v+1}{v(v+1)} L_v(\theta_0 + \theta_1) \cdot$$

$$L_v'(\mu) [L_v'(\mu_0)]^{-2} \frac{\partial v}{\partial \mu_0} \left[\frac{M_v(\beta_0 a) J_v(\beta_0 R) - M_v(\beta_0 R) J_v(\beta_0 a)}{M_v(\beta_0 a)\ J_v'(\beta_0 b)}\right] \tag{1-69c}$$

The magnetic field can be decomposed into three parts. Thus, $(B_\Phi^I)_{1D}$ is the contribution solely from the dominant modes inside the antenna region, whereas $(B_\Phi^I)_{1C}$ represents essentially the contributions from the complementary modes and $(B_\Phi^I)_{1E}$ the contributions due to the presence of central sphere. It is noted that $(B_\Phi^I)_{1E}$ vanishes when the

inner sphere is shrunk to zero. However, the identification of $(B_\Phi^I)_{1E}$ with the inner sphere is not entirely clear-cut since the b_k's involved in $(B_\Phi^I)_{1D}$ and $(B_\Phi^I)_{1C}$ have already taken account of the effect of the inner sphere in the solution of the infinite set of linear equations.

Similarly, substitution of (1-37), (1-39a), (1-51) and (1-52) into (1-40a) and (1-40b) gives

$$(E_\vartheta^I)_1(\theta, R) = (E_\theta^I)_{1D} + (E_\theta^I)_{1C} + (E_\theta^I)_{1E} \tag{1-70a}$$

where

$$(E_\theta^I)_{1D} = \frac{\xi_0 V_0^e}{2\pi R Z_c \sin\theta} [\cos\beta_0 R_b + \tan\beta_0 h \sin\beta_0 R_b - \frac{j 120 \sin\beta_0 R}{Z_c \cos\beta_0 h} \sum_k{}' \frac{b_k}{k(k+1)} P_k(\theta_0)] \tag{1-70b}$$

$$(E_\theta^I)_{1C} = \frac{-j \xi_0 \sin\theta V_0^e}{2\pi R} [\sum_k{}' \sum_v \frac{2v+1}{v(v+1)} \frac{P_k(\theta_0)}{[k(k+1) - v(v+1)} \frac{L_v'(\mu)}{L_v'(\mu_0)} \frac{M_v'(\beta_0 R)}{M_v(\beta_0 a)} \frac{\partial v}{\partial \mu_0} b_k] \tag{1-70c}$$

$$(E_\theta^I)_{1E} = \frac{\sin\theta V_0^e}{2R(1-\mu_0^2)} \frac{1}{fn(\theta_0, \theta_1)} \sum_v \frac{2v+1}{v(v+1)} L_v(\theta_0 + \theta_1) L_v'(\mu) [L_v'(\mu_0)]^{-2} \frac{\partial v}{\partial \mu_0} [\frac{M_v(\beta_0 a) J_v'(\beta_0 R) - M_v'(\beta_0 R) J_v(\beta_0 a)}{M_v(\beta_0 a) J_v(\beta_0 b)}] \tag{1-70d}$$

and

$$(E_R^I)_1(R, \theta) = (E_R^I)_{1C} + (E_R^I)_{1E} \tag{1-71a}$$

where

$$(E_R^I)_{1E} = \frac{V_0^e}{2(1-\mu_0^2)\beta_0 fn(\theta_0,\theta_1) R^2} \sum_v \frac{(2v+1) L_v(\theta_0+\theta_1)}{[L_v'(\mu_0)]^2} \frac{\partial v}{\partial \mu_0}$$

$$\left[\frac{M_v(\beta_0 a) J_v(\beta_0 R) - J_v(\beta_0 a) M_v(\beta_0 R)}{M_v(\beta_0 a) J_v'(\beta_0 b)}\right] \qquad (1-71b)$$

$$(E_R^I)_{1C} = \frac{j}{2\pi\omega\epsilon_0 R} \sum_k' \sum_v \frac{(2v+1)}{[k(k+1) - v(v+1)]} \frac{M_v(\beta_0 R)}{M_v(\beta_0 a)} P_k(\theta_0)$$

$$\frac{\partial v}{\partial \mu_0} \frac{b_k}{L_v'(\mu_0)} \qquad (1-71c)$$

By the same procedures, the corresponding expressions for the electromagnetic fields in region I associated with the second set of equations may be obtained by substituting (1-37), (1-39a), (1-60) and (1-61) in (1-40a-c) separately. Comparisons between corresponding formulae for the first and second sets of equations show that with a simple replacement of terms, the fields for the second set of equations can easily be obtained from formulae for the first set of equations and vice versa according to the following rules; i.e.,

E-M Fields for 1st Set	E-M Fields for 2nd Set
b_k	$b_k \rho_k(\beta_0 a)$
$\beta_0 h$	$\pi/2 + \beta_0 h$
$M_v(\beta_0 a)$	$M_v'(\beta_0 a)$
$J_v(\beta_0 a)$	$J_v'(\beta_0 a)$

(1-72)

(v) Current Distribution

Distributions of currents over the surfaces of the modified dipole structure are obtained from the boundary condition (1-66). The boundary condition $n \cdot B = 0$ is satisfied automatically since it is obvious from the

fact that the only currents excited in the present case are I_R along the conical surface and I_θ on the surface of the conical cap and the inner sphere.

The currents on the different parts of the antenna for the first set of equations [formulae for the second set can easily be obtained by using (1-72)] may be expressed as follows:

Along the surfaces of inner sphere:

Current density

$$I_{ds}(b,\theta) = [(I_{ds})_{1D} + (I_{ds})_{1C} + (I_{ds})_{1E}]\,\theta$$
$$= \nu_0 [(B^I_\Phi)_{1D}(b,\theta) + (B^I_\Phi)_{1C}(b,\theta) + (B^I_\Phi)_{1E}(b,\theta)]\theta \qquad (1-73)$$

Total current

$$I_{ts}(b,\theta) = [(I_{ts})_{1D} + (I_{ts})_{1C} + (I_{ts})_{1E}]\,\theta$$
$$= 2\pi b \sin\theta\, I_{ds}(b,\theta) \qquad (1-74)$$

Along the surfaces of the conical dipole:

Current density

$$I_{dc}(R,\theta_0) = [(I_{dc})_{1D} + (I_{dc})_{1C} + (I_{dc})_{1E}]\,R$$
$$= \nu_0 [(B^I_\Phi)_{1D}(R,\theta_0) + (B^I_\Phi)_{1C}(R,\theta_0) + (B^I_\Phi)_{1E}(R,\theta_0)]\,R \qquad (1-75)$$

Total current

$$I_{tc}(R,\theta_0) = [(I_{tc})_{1D} + (I_{tc})_{1C} + (I_{tc})_{1E}]\,R$$
$$= 2\pi R \sin\theta_0\, I_{dc}(R,\theta_0) \qquad (1-76)$$

Along the surfaces of the conical cap:
Current density

$$I_{dp}(a,\theta) = [(I_{dp})_{1D} + (I_{dp})_{1C} + (I_{dp})_{1E}]\,\theta$$
$$= \nu_0 [(B^I_\Phi)_{1D}(a,\theta) + (B^I_\Phi)_{1C}(a,\theta) + (B^I_\Phi)_{1E}(a,\theta)]\,\theta \quad (1\text{-}77)$$

Total current

$$I_{tp}(a,\theta) = [(I_{tp})_{1D} + (I_{tp})_{1C} + (I_{tp})_{1E}]\,\theta$$
$$= 2\pi a \sin\theta\, I_{dp}(a,\theta) \quad (1\text{-}78)$$

(vi) Input Admittance

The input admittance of the modified dipole is defined in the following manner. Over the circular gap at R = b between conical antenna and inner sphere exists an electric potential V_0, i.e.,

$$V_0 = \int_{\theta_0}^{\theta_0+\theta_1} E_\theta\, b\, d\theta = \frac{V^e_0}{2} \quad (1\text{-}79)$$

From (1-76), the total current in the antenna at the driving point, i.e., at R = b, is given by:

$$I_0 = I_{tc}(b,\theta_0) = 2\pi\nu_0 b \sin\theta_0 (B^I_\Phi)(b,\theta_0) \quad (1\text{-}80)$$

The terminal admittance at R = b is then defined by

$$Y_0 = \frac{I_0}{V_0} \quad (1\text{-}81)$$

More explicitly,

$$Y_0 = Y_{1D} + Y_{1C} + Y_{1E} \quad (1\text{-}82)$$

where

$$Y_{1D} = \frac{2}{Z_c}\left[j \tan\beta_0 h + \frac{120}{\cos\beta_0 h} \sum_k{}' \frac{b_k}{k(k+1)} P_k(\theta_0)\right] \tag{1-83a}$$

$$Y_{1C} = -2(1-\mu_0^2) \sum_k{}' \sum_v \left[\frac{(2v+1)}{v(v+1)} \cdot \frac{P_k(\theta_0)}{k(k+1) - v(v+1)} \cdot \right.$$

$$\left. \frac{M_v(\beta_0 b)}{M_v(\beta_0 a)} \cdot \frac{\partial v}{\partial \mu_0}\right] b_k \tag{1-83b}$$

$$Y_{1E} = \frac{-j}{60\, fn(\theta_0, \theta_1)} \sum_v \left[\frac{(2v+1)}{v(v+1)} \frac{L_v(\theta_0, \theta_1)}{L_v'(\mu_0)} \frac{\partial v}{\partial \mu_0} \cdot \right.$$

$$\left. \frac{M_v(\beta_0 a)\, J_v(\beta_0 b) - M_v(\beta_0 b)\, J_v(\beta_0 a)}{M_v(\beta_0 a)\, J_v'(\beta_0 b)}\right] \tag{1-83c}$$

(vii) Far-field Pattern

The far electromagnetic field in the radiation region II is easily obtained by substituting the asymptotic form of the Hankel function of the second kind in (1-44a, c), i. e.,
let $R \to \infty$

$$R_k(x) = x\, h_k^{(2)}(x)$$

$$\approx \exp\left[-j\left(x - \frac{k+1}{2}\pi\right)\right] \tag{1-84}$$

and

$$R_k'(x) = h_k^{(2)}(x) + x\, h_k^{(2)'}(x)$$

$$\approx \frac{-j}{x} \exp\left[-j\left(x - \frac{k+1}{2}\pi\right)\right] \tag{1-85}$$

So

$$E_\theta^{II} \approx \frac{-\xi_0 \exp(-j\beta_0 R)\, V_0^e}{2\pi R} F(\theta) \tag{1-86}$$

$$B_{\phi}^{II} \sim \frac{-\exp(-j\beta_0 R)\, V_0^e}{2\pi\nu_0 R} F(\theta) \qquad (1\text{-}87)$$

where $F(\theta)$ is the radiation factor

$$F(\theta) = \sum_k{}' \frac{b_k}{k(k+1)} \frac{P_k'(\theta)}{R_k(\beta_0 a)} (-1)^{\frac{(k+1)}{2}} \qquad (1\text{-}88)$$

The radiation factor is zero at $\theta = 0$. The far field should decay as $1/R$. If the field decays faster than $1/R$ in a certain direction, the radiation pattern must have a zero in that direction. On the other hand, if the field decays slower than $1/R$, then the radiation pattern should be infinite in that direction as in the case of an infinite cylindrical antenna. The far-field radiated power is

$$P = \frac{1}{2} \int_0^{\pi} E_{\theta} \times H_{\Phi}^{*}\, 2\pi R^2 \sin\theta\, d\theta$$

$$= 60(V_0^e)^2 \sum_k{}' \frac{|b_k|^2}{(2k+1)\, k(k+1)} \frac{1}{|R_k(\beta_0 a)|^2} \qquad (1\text{-}89)$$

(3) Biconical Antenna

An important limiting case of the modified conical dipole is when the radius of inner sphere approaches zero. In this case, it becomes a symmetrically excited biconical antenna. This is of special interest in the present case. One of the modifications made in formulating the theoretical approach was to replace the thin cylindrical antenna protruding out from a conducting sphere with a thin conical antenna under the assumption that in the limit (i. e., cone angle becomes small), their performances should become reasonably the same. A rigorous theoretical formulation for the input impedance of a biconical antenna was obtained by Tai [1], and extensive knowledge of the cylindrical

antenna is also available [1]-[2]. Therefore, one would expect that a comparison of the properties of conical and cylindrical antennas would serve as a convenient way of studying the validity of the above-mentioned modification in the theoretical treatment. Furthermore, since the limiting results obtained for the modified dipole with a shrinking inner sphere correspond to those for the biconical dipole, this latter serves as a check on the internal consistency and accuracy of the numerical calculations.

First, we will list below the infinite set of linear equations and the general solution for the infinite set of linear equations and the general solution for the input impedance of the biconical dipole obtained by Tai (see Fig. 1-4). The infinite set of linear equations is

$$\frac{\rho_r(\beta_0 h)}{2r+1}\, d_k + r(r+1)\, P_r(\theta_0) \sum_k{}' \sum_v \Phi(v, r, k)\, P_k(\theta_0)\, d_k = -\, P_r(\theta_0) \qquad (1\text{-}90)$$

$$(r = 1, 3, 5, \ldots)$$

where

$$\Phi(v, r, k) = \frac{2v+1}{v(v+1)} \frac{(1-\mu_0^2)}{[k(k+1) - v(v+1)]\,[r(r+1) - v(v+1)]} \cdot \frac{\partial v}{\partial \mu_0} \frac{J_v'(\beta_0 h)}{J_v(\beta_0 h)} \qquad (1\text{-}91)$$

and

$$d_k = \frac{b_k}{I_m} \qquad (1\text{-}92)$$

The d_k's are the complex coefficients for the electromagnetic field in the radiation region II, and I_m is a constant defined by

$$I_m = \frac{j\, V_0^e}{Z_c(\cos\beta_0 h + j Z_c Y_{1a} \sin\beta_0 h)} \qquad (1\text{-}93)$$

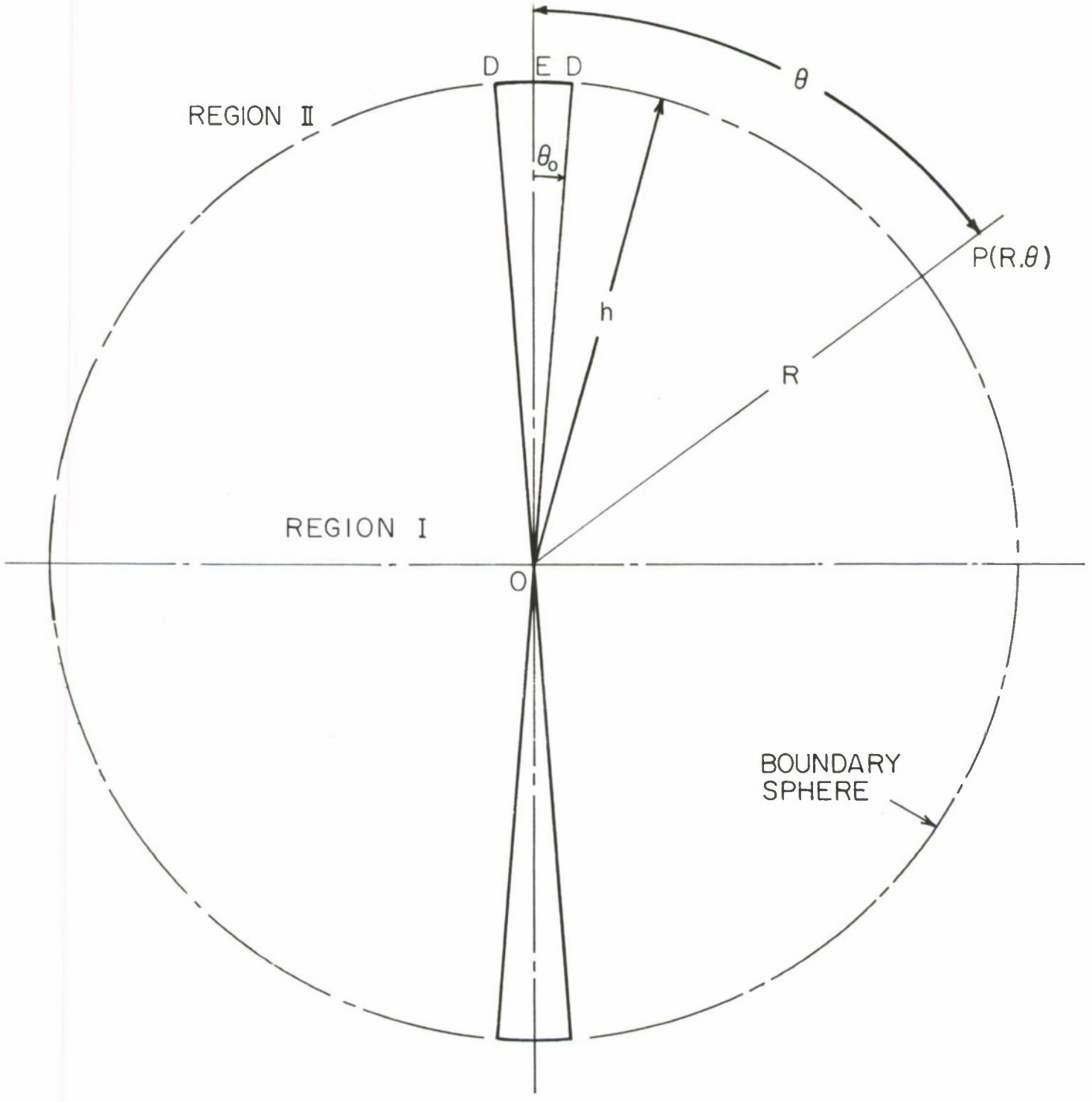

FIG. 1-4 THIN BICONICAL ANTENNA

Note that I_m is the maximum current. When $Y_{1a} = 0$, $I_m = I_0/\sin\beta_0 h$ at $R = h - \lambda_0/4$ (which corresponds to $I_m = I_0/\sin\beta_0 h$ at $Z = h - \lambda_0/4$ for the cylindrical antenna with sinusoidally distributed current), and Y_{1a} is the apparent dominant-mode terminal admittance which is defined as follows

$$Y_{1a} = (R^e_{mc} + jX^e_{mc})/(Z_c)^2$$

$$= \frac{j\xi_0}{\pi Z_c^2} \sum_k{}' \frac{1}{k(k+1)} d_k P_k(\theta_0) \qquad (1\text{-}94)$$

By analogy with Y_{1a} for the two-wire line with end effects, Y_{1a} is the apparent load at the end of the biconical transmission line if only dominant-mode current and voltage are considered.

The driving point impedance Z_0 is

$$Z_0 = R_0 + jX_0$$

$$= Z_c \left(\frac{Z^e_{mc}\sin\beta_0 h - jZ_c\cos\beta_0 h}{Z_c\sin\beta_0 h - jZ^e_{mc}\cos\beta_0 h}\right) \qquad (1\text{-}95)$$

With some necessary modifications, formulations for the symmetric center-fed biconical antenna are derived in a manner almost equivalent to that leading to (1-57) and (1-64) of the modified dipole. Note that: (1) Since the origin is now included, Bessel's functions of the second kind which have a singularity at $R = 0$ must be excluded. This is equivalent to setting the arbitrary constants b_v's equal to zero in (1-25a-c). (2) As noted for the modified dipole in (1-37), the arbitrary constant a'_0 for the dominant modes is quite insensitive to the way in which the antenna is being driven. It is uniquely determined by the driving voltage as well as the conical shape. On the other hand, the arbitrary constants (i.e., a'_vs and b'_vs) for the complementary modes are closely dependent upon how the antenna is driven. This dependence, however, becomes less significant as the radius of the inner sphere becomes smaller until finally, when b becomes zero, complementary

modes play no role at the driving point. This can easily be seen by checking the leading term of the complementary modes of E_θ at a very small radial distance δ from the apex, i.e.,

$$(E^I_\theta)_{v/0} \approx 2\beta_0^2 L'_{v_1}(\theta) a'_{v_1} \frac{(v_1+1)2^{v_1}\Gamma(v_1+1)}{\Gamma(2v_1+2)} (\beta_0\delta)^{v_1-1}$$

$$\approx (\beta_0\delta)^{v_1-1} \tag{1-96}$$

where v_1 is the smallest root of the characteristic equation $L_v(\theta_0) = 0$.

As will be seen later, in the range of interest v_1 is always greater than unity. Therefore, at the apex (b = 0), the driving condition (1-34) can still be used without loss of generality. The whole system (b = 0) is now insensitive to the way it is driven and only the total driving voltage and the shape of the cone are significant. Accordingly, carrying out the same procedures as used for the modified dipole, one obtains the following for the biconical antenna:

(a) Infinite Set of Linear Equations

(i) First set of linear equations ($\beta_0 h \neq \pi/2, 3\pi/2, \ldots$)

$$\sum_k{}' (C_{rk})_b b_k = -D_r \tag{1-97}$$

where

$$(C_{rk})_b = V_{rk} + (E_{rk})_b - \delta_{rk} B_{rk} \tag{1-98a}$$

$$(E_{rk})_b = -2(1-\mu_0^2) P_r(\theta_0) P_k(\theta_0) \sum_v \left[\frac{(2v+1)}{v(v+1)} \cdot \frac{J'_v(\beta_0 h)}{J_v(\beta_0 h)} \cdot \frac{1}{[k(k+1)-v(v+1)][r(r+1)-v(v+1)]} \frac{\partial v}{\partial \mu_0} \right] \tag{1-98b}$$

and D_r, V_{rk} and B_{rk} in (1-97) are identically the same as those given in (1-57a) and (1-58d) with the substitution of h for a in those equations.

(ii) Second set of linear equations

$$\sum_k{}' \, (C'_{rk})_b \, b_k = - D'_r \tag{1-99}$$

where

$$(C'_{rk}) = D'_{rk} + V'_{rk} + (E'_{rk})_b - \delta_{rk} \, B'_{rk} \tag{1-100a}$$

and

$$(E'_{rk})_b = - 2(1 - \mu_0^2) \, \rho_k(\beta_0 h) \, P_r(\theta_0) \, P_k(\theta_0) \sum_v \left[\frac{(2v+1)}{v(v+1)} \cdot \right.$$

$$\left. \frac{J_v(\beta_0 h)}{J'_v(\beta_0 h)} \, \frac{\frac{\partial v}{\partial \mu_0}}{[k(k+1) - v(v+1)][r(r+1) - v(v+1)]} \right] \tag{1-100b}$$

and D'_r, D'_{rk}, V'_{rk}, and B'_{rk} are the same as those given in (1-65a) and (1-65d) with the substitution of h for a in those equations.

Comparing the corresponding infinite sets of linear equations for the modified dipole and the conical dipole, one observes that the latter can easily be derived from the former by taking the asymptotic limit (i.e., $b \to 0$). An extra source term (i.e., D_{r2} for the first set and D'_{r2} for the second set) which is a function of both θ_0 and θ_1, has been added to the formulation for the modified dipole to take account of the inner conducting sphere. Two quantities are of special interest since they serve as convenient parameters for studying the effects of the central sphere on the performance of the dipole antenna. One of them is $A_v = M_v(\beta_0 a) \, J_v(\beta_0 b)$ for the first set or $A'_v = M'_v(\beta_0 a) \, J'_v(\beta_0 b)$ for the second set. Both A'_v and A_v approach infinity as the radius b of the sphere becomes smaller. Hence the importance of the second source term (i.e., D_{r2} or D'_{r2}) decreases for a shrinking radius b. The other quantity is $B_v = M'_v(\beta_0 a)/M_v(\beta_0 a)$ for the first set or $B'_v = 1/B_v$ for the second set.

In the limit as $b \to 0$,

$$B_v \approx \frac{J'_v(\beta_0 a)}{J_v(\beta_0 a)} \qquad \text{and} \qquad B'_v \approx \frac{J_v(\beta_0 a)}{J'_v(\beta_0 a)}$$

which implies that $E_{rk} \to (E_{rk})_b$ and $E'_{rk} \to (E'_{rk})_b$ which makes the coefficient matrix of the modified dipole approach that of the conical antenna. So the difference between B_v and J'_v/J_v also measures the effect of the central sphere.

Accordingly, formulae for the current distribution and the input admittance for the biconical dipole can also be conveniently obtained by taking the asymptotic limit of the corresponding equations for the modified dipole.

(b) Electromagnetic Field in Region I

$$(B^I_\Phi)_1(\theta, R) = (B^I_\Phi)_{1D} + (B^I_\Phi)_{1C} \tag{1-101}$$

where

$$(B^I_\Phi)_{1D} = \frac{V^e_0}{2\pi \nu_0 Z_c R \sin\theta} \left[-j(\sin\beta_0 R - \cos\beta_0 R \tan\beta_0 h) + \frac{120 \cos\beta_0 R}{\cos\beta_0 h} \sum_k{}' \frac{b_k}{k(k+1)} P_k(\theta_0)\right] \tag{1-102a}$$

$$(B^I_\Phi)_{1C} = \frac{-\sin\theta\ V^e_0}{2\pi \nu_0 R} \sum_k{}' \sum_v \left[\frac{(2v+1)}{v(v+1)} \frac{P_k(\theta_0)}{[k(k+1) - v(v+1)]} \cdot \frac{L'_v(\mu)}{L'_v(\mu_0)} \frac{\hat{J}_v(\beta_0 R)}{\hat{J}_v(\beta_0 h)} \frac{\partial v}{\partial \mu_0} b_k\right] \tag{1-102b}$$

$$(E^I_\vartheta)_1(\theta, R) = (E^I_\theta)_{1D} + (E^I_\theta)_{1C} \tag{1-103}$$

where

$$(E^I_\theta)_{1D} = \frac{\xi_0 V^e_0}{2\pi R Z_c \sin\theta} \left[\cos\beta_0 R + \tan\beta_0 h \sin\beta_0 R - \frac{120 \sin\beta_0 R}{Z_c \cos\beta_0 h} \sum_k{}' \frac{b_k}{k(k+1)} P_k(\theta_0)\right] \tag{1-104a}$$

$$(E^I_\theta)_{1C} = \frac{-j\xi_0 \sin\theta\ V_0^e}{2\pi R} \sum_k{}' \sum_v \left[\frac{(2v+1)\ P_k(\theta_0)}{[k(k+1) - v(v+1)]\ v(v+1)} \cdot \right.$$

$$\left. \frac{L'_v(\mu)}{L'_v(\mu_0)} \frac{J_v(\beta_0 R)}{J_v(\beta_0 a)} \frac{\partial v}{\partial \mu_0} b_k \right] \qquad (1\text{-}104b)$$

and

$$(E^I_R)_1(\vartheta, R) = (E^I_R)_{1C}$$

$$= \frac{j}{2\pi\omega\epsilon_0 R^2} \sum_k{}' \sum_v \left[\frac{2v+1}{[k(k+1) - v(v+1)]} \frac{J_v(\beta_0 R)}{J_v(\beta_0 a)} \cdot \right.$$

$$\left. \frac{P_k(\theta_0)}{L'_v(\theta_0)} \frac{\partial v}{\partial \mu_0} b_k \right] \qquad (1\text{-}105)$$

Note that all the terms associated with the central sphere vanish. The fields for the second set of equations can easily be obtained from formulae for the first set of equations by using (1-72).

(c) Input Admittance

The driving voltage is now defined as

$$V_0 = \int_{\theta_0}^{\pi-\theta_0} E_\theta\ b\ d\theta = V_0^e \qquad (1\text{-}106)$$

Hence the input admittance is

$$(Y_0)_1 = \frac{1}{Z_c} \left[j \tan\beta_0 h + \frac{120}{\cos\beta_0 h} \sum_k{}' \frac{b_k}{k(k+1)} P_k(\theta_0) \right]$$

$$(\beta_0 h \neq \pi/2,\ 3\pi/2, \ldots) \qquad (1\text{-}107)$$

or

$$(Y_0)_2 = \frac{1}{Z_c} \left[-j\cot\beta_0 h - \frac{120}{\sin\beta_0 h} \sum_k{}' \frac{\rho_k(\beta_0 h)}{k(k+1)} P_k(\theta_0) \right]$$

$$(\beta_0 h \neq \pi,\ 2\pi, \ldots) \qquad (1\text{-}108)$$

where subscripts 1 and 2 denote the first and second sets of linear equations respectively.

(C) Driving by a Radial Delta-Function

It has been shown by Chang [15] that the same integral equations, hence the same current distribution, obtained for a tubular dipole excited either by an axial delta-function generator or by a radial delta-function generator on the outside surface of the antenna. Further studies have been carried out when a radial $1/\rho$ excitation is used instead of the radial delta-function generator. It has been found that both theoretical models give a satisfactory description of the current behavior away from the driving point. However, near the driving point, the model with the delta-function driving gives a logarithmically increasing current, while the model with a finite gap excitation gives a finite current and remains in good agreement with the experimental measurement. Therefore, in this section for the purpose of comparison, the formulation for the modified dipole will be carried out when this is excited by a radial delta-function excitation. Only (1-34) describing the driving condition has to be modified to account for the delta-function source, namely,

$$(E_\theta^I)_{R=b} = \frac{V_0^e}{2b} [\delta(\theta - \theta_0) + \delta(\theta - \pi + \theta_0)] \tag{1-109}$$

where $V_0^e/2$ is the voltage maintained across the infinitely small gap. Again, the arbitrary constant a_0' is still determined uniquely by the driving voltage and the cone shape, while the relation between the arbitrary constants a_ν' and b_ν' differs only by a slight modification of the constant a_ν. Thus,

$$a_\nu = \frac{- V_0^e L_\nu'(\mu_0)(1 - \mu_0^2)}{2\beta_0 \nu(\nu+1) J_{\nu\nu} J_\nu(\beta_0 b)} \tag{1-110}$$

In carrying out the derivation of the infinite set of linear equations, one observes that the only difference from those for the finite gap occurs in the second driving-source term. Therefore, a simple modification in the source term gives the formulation for the delta-function generator. The quantity in question is [from (1-58c)],

$$C_v = \frac{-L_v(\theta_0 + \theta_1)}{(1-\mu_0^2)\, L_v'(\mu_0)\, \mathrm{fn}(\theta_0, \theta_1)}$$

In the case of the delta-function generator,

$$\lim_{\theta_1 \to 0} C_v \approx 1 \qquad (1\text{-}111)$$

Therefore, the quantity C_v has the special function of measuring the effect of the width of the gap.

In short, the presence of the central sphere is well represented in the second source term, i. e., C_v/A_v. A_v accounts for the size of the sphere while C_v takes into account the driving gap. Therefore, in the case of the vanishing sphere, $A_v \to \infty$, the second source term is relatively much smaller than the first source term. Hence, the effect of C_v is also greatly affected through the vanishingly small factor $1/A_v$. In other words, the whole system is now insensitive to the method of driving. Generally speaking, C_v is a relatively slowly-varying function with respect to θ_1. For narrow-gap driving, it has little or no effect upon the field in the radiation region. In the actual numerical calculation, it has been found that for driving gap as large as 2.5^o, C_v differs from 1 by 10^{-3}. This means that it is possible to set $C_v = 1$ in solving the infinite set of linear equations without introducing any appreciable errors provided the gap is not large. It is also instructive to note that in the formula for the admittance, only Y_{1E} is affected by the gap width, and it is an imaginary quantity. Therefore, the effect of driving gap will only appear in the input susceptance.

B. EXPERIMENTAL STUDY

1. INTRODUCTION

In the preceding section (and later in Volume II), it is established that: (i) With an appropriate average characteristic impedance, the theoretical performance of a conical antenna is quite comparable to that of the cylindrical dipole which has been studied extensively and thoroughly [2] both in theory and experiment. On the other hand, it is difficult to drive the thin conical antenna with a coaxial line without introducing significant complementary-mode currents into the definition of the impedance of the cone. The experimental difficulty arises primarily in the complexity of the analysis of the effect of the terminal zone near the junction of the line and antenna. Therefore, little quantitative information is available except for wide-angle cones [12]. (ii) Except for very small central modifications, the performance of a modified conical dipole differs significantly from that of a corresponding thin conical dipole. But the latter serves as an extrapolatory check for the former with a vanishing central sphere.

Therefore, the purpose of this experimental study is to establish the adequacy of the theory of the modified conical dipole just presented for a representative set of antennas and central modifications included within the scope of the theory, and then to compare experimentally the performance of the modified conical dipole with the corresponding modified cylindrical antenna to justify the approximation made in the theoretical treatment in replacing a cylindrical antenna by a conical one.

The experimental difficulty encountered with a simple conical dipole is somewhat reduced in the case of the modified conical antenna due to the fact that the driving condition has been changed from an experimentally unattainable point generator to a quite well-understood coaxial line feed. By determining the apparent load impedance as seen from the coaxial line together with a proper terminal correction, a measurable quantity is defined.

As was observed in the preceding section the formulae for the biconical antenna are actually the asymptotic forms of those for the modified conical antenna with a shrinking central sphere. Also, numerical results presented in Volume II suggest that the performance of the modified conical dipole with a small central sphere comes quite close to that of a biconical antenna. Therefore, the present experiments also serve as an indirect experimental check for the biconical antenna for which generators that are equivalent to a singularity with electric field do not exist and are difficult to approximate.

In this experimental study, it was considered essential to observe the current distribution ober the entire antenna structure as well as the terminal properties i. e. , the input admittance or impedance. The measurement of the radiation pattern was not considered of fundamental importance since the correlation between experimental and theoretical current distributions constitute a more critical measure of the validity of the theory than the radiation patterns. Due to the technical difficulty in preparing a set of metal hemispheres with various sizes, the experiment was performed on a fixed installation for which only the frequency and antenna length could be varied. The operating frequency range in this experiment was chosen to be 100-600 MHz with a corresponding free-space wave length of 300 cm to 50 cm so that even with one hemisphere (b = 12. 4 cm), it was possible to obtain various central modifications ($\beta_0 b$ = 0. 31-1. 51) covering the whole range of interest. The physical size of the antenna that was under test was chosen to range from 10 cm to 60 cm with a half cone angle θ = 1. 1°. As a result of the previous theoretical analysis, the performance of the cone is known to change drastically as the central sphere becomes larger. Therefore, a relatively large physical size of the hemisphere was chosen so that an electrically large hemisphere would fall in the neighborhood of the frequency 500 MHz for which the original image screen was designed [18]. In this manner less experimental error was introduced and a more critical comparison between experiment and theory could be achieved.

2. ANTENNA STRUCTURE

The physical configuration used was intended to represent as closely as possible the mathematical model involved in the theory. The theoretical conical transmission line was replaced by a coaxial line. In Fig. 1-5, is shown the cross-sectional view of the experimental antenna structure with dotted lines added to represent the corresponding mathematical model. The modified antenna structure consists of a hemisphere, a coaxial measuring line which penetrates the ground plane and goes to a hole in the hemisphere where the outer conductor is attached to the conducting spherical surface and a removable conical antenna of various lengths is connected to the inner conductor of the coaxial line. The coaxial line spacing produces an annular gap at the end of the radial hole, the antenna is driven by the fields in the region and hence the input admittance is also defined here. The fact that this annular gap is a very good, though not perfect, representation of the conical transmission line can be seen in Fig. 1-5b where the driving part has been much exaggerated for purposes of explanation. For small angles θ_0 and θ_1, the transverse electric field maintained by the TEM mode in a coaxial line is inversely proportional to radial distance from the axis, i.e.,

$$E\rho \propto 1/\rho \tag{1-112}$$

while for conical transmission line, E_θ is inversely proportional to $\sin\theta$ (angle in spherical coordinates) i.e.,

$$E_\theta \propto 1/\sin\theta \tag{1-113a}$$

or

$$\propto 1/(b\theta) \qquad \text{for small } \theta \tag{1-113b}$$

The fact that θ_0 and θ_1 are small implies that side QQ' which is approximately equal to $(a_2-a_1)\theta_0$ is negligible as compared to (a_2-a_1). So the two sides PQ and PQ' are practically coincident. Hence E_ρ is indeed a good representation of E_θ. A photograph showing an overall view of the hemisphere with a conical antenna mounted is in Fig. 1-6.

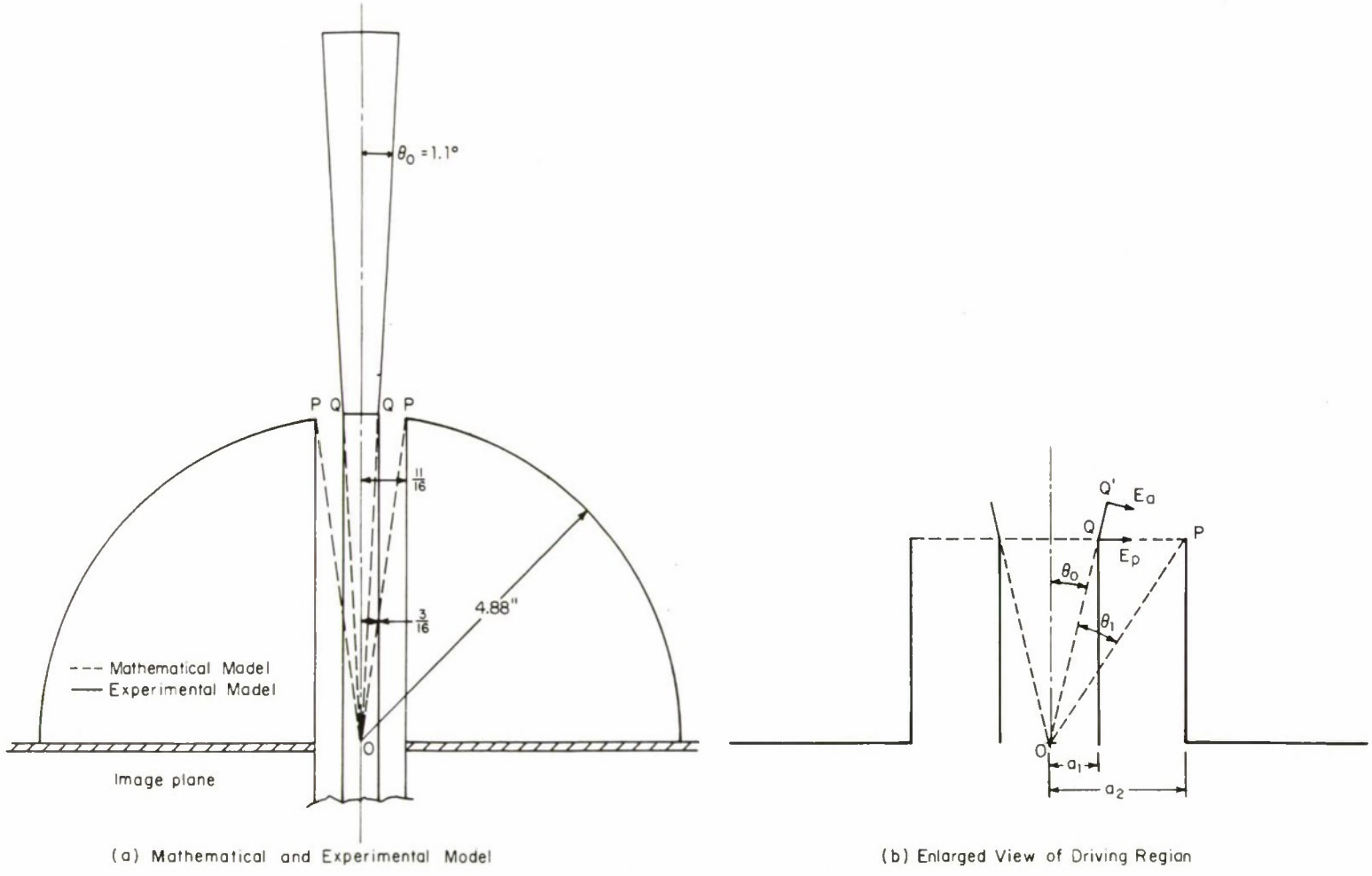

FIG. 1-5 MATHEMATICAL AND THEORETICAL MODEL OF MODIFIED CONICAL ANTENNA

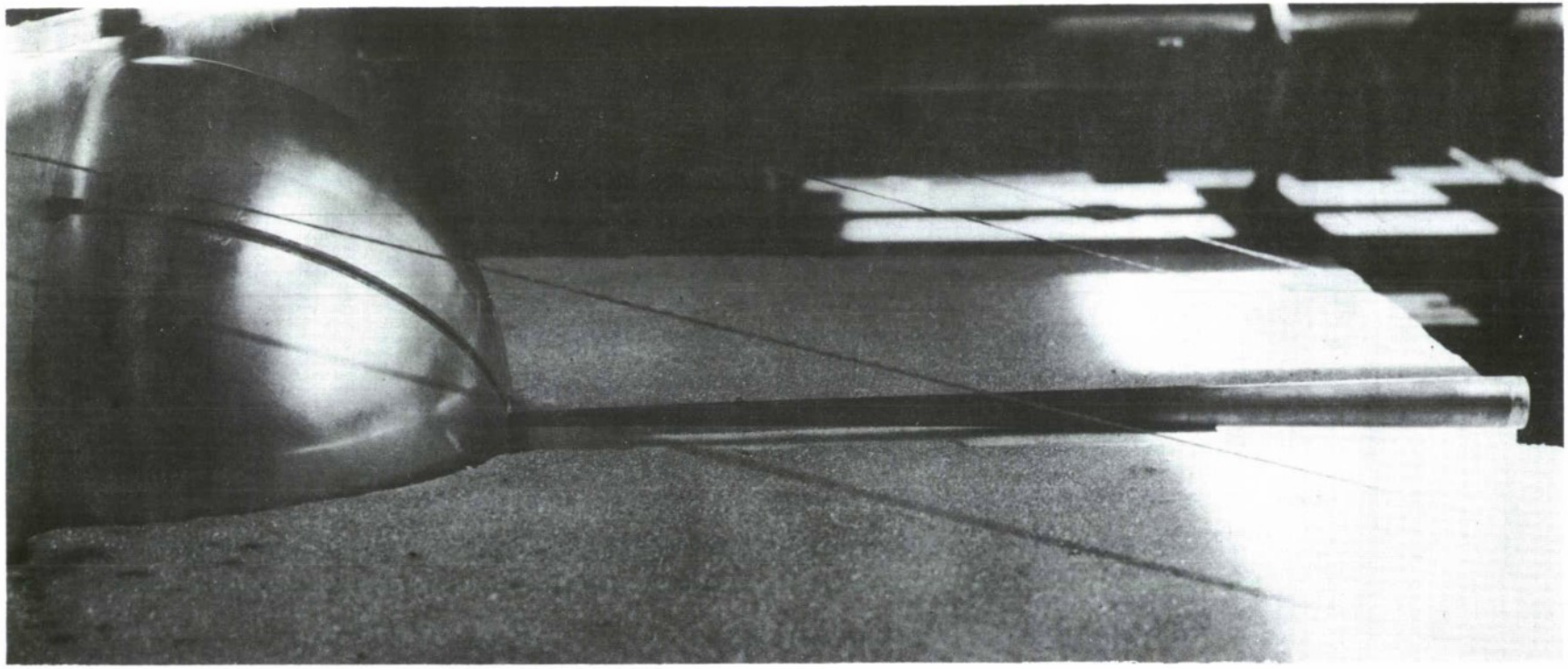

FIG. 1-6 EXPERIMENTAL MODEL OF MODIFIED CONICAL DIPOLE

The size of the antenna structure depends largely upon what is available in the commercial market and upon the range of parameters, to be covered. In order to obtain a sphere with electrical radii ranging from $\beta_0 b = 0.3$ to 1.5 in the operating frequency range of 100-600 MHz, the radius of the sphere should be about 5 inches. The smallest available size of hollow brass tubing (which should, however, be large enough to accommodate the motion of current probes) has the outside diameter (OD) $\frac{3}{16}''$ and inside diameter (ID) $\frac{1}{8}''$. Once the size of the inner conductor was chosen to obtain a conical antenna with half angle 1.1° (which value is selected so that the available theoretical data can be used for comparison directly) the size of the sphere turned out to be one with radius 4.88'' which was exactly in the desired range. Again, the choice of the outer conductor of the coaxial line to make the annular gap formed present an angle of 1.5° with respect to the origin, required a brass tube with ID $\frac{5}{8}''$ and OD $\frac{11}{16}''$. The characteristics of the measuring line will be discussed later.

Due to the shape of the conical antenna, it is difficult to construct a model with continuous variation in height. Instead, antennas were built with lengths varying in the form of steps. The stepwise variation in height was chosen small enough to provide sufficient experimental data. Because of the small cone angle, the cone antennas of shorter length with small end caps were carefully machined from a solid brass rod. A radial slot of width $\frac{1}{32}''$ was formed along the conical surface. The slot enables the exploration of current distribution along the antenna by means of probes mounted inside a tube which is embedded along the conical surface. The probe is of the same size as the inner conductor of the coaxial line so that the probes used in the antenna can also be used for the coaxial line. The lengths of the antennas actually constructed range from 10 cm up to 35 cm in steps of 2.5 cms. As the antenna became longer, the cap surface was soon large enough to allow machining. Thus, for the longer cone antenna (> 35 cm), sets of short section were made, each 2.5 cm in height, with continuous variation in width in conformity with the shape of the cone antenna. These sections could be added successively to the longest brass antenna (h = 35 cm) to make still longer ones. Thus,

the longest antenna is 60 cm. In Fig. 1-7, are shown photographs of the conical antennas.

The conical antenna is mounted on the inner conductor of the coaxial line at the driving point, through a rather fragile but effective connection shown in Fig. 1-8b, in which the inner wall of the conducting tube was reduced to 1/64'' by removing 1/64'' from the outside. The connecting section of the conical antenna was also reduced to 11/64'' by removing 1/64'' from the inside. The longitudinal slot along the coaxial line was aligned to the radial slot of the conical antenna so that probes could be moved freely from the coaxial line to the antenna. A set of cylindrical antennas (with lengths 20 cm, 30 cm, 50 cm) with the same radius as the inner conductor were prepared. Three pieces were quite enough since the inner conductor itself could be extended to function as a monopole antenna.

Slots were also cut along the spherical surface in a plane containing the antenna so that a small shielded loop probe could be moved along a circumference by pulling the attached cable by means of a carriage on a rack behind the ground plane (Fig. 1-8a).

The metal hemisphere was bolted to a removable antenna mounting plate which was permanently attached to a movable horizontal coaxial line. The line was attached to the hemisphere through a mating flange near the ground plane.

3. MEASURING LINE

(A) Mechanical Characteristics

The measuring line, the tubes for positioning the antenna and probes were patterned largely after those constructed by Mack [19], Simpson [20] and to some extent, after that of Andrews [18]. The design of the probes used to explore the distribution of current and voltage along the line (as well as the current on the entire antenna structure) followed the work of Whiteside [21]. A schematic diagram showing the essential features in the construction of the measuring line is in Fig. 1-9. The entire measuring line is mounted on an 11 ft. long and 1-1/2 in. thick plywood

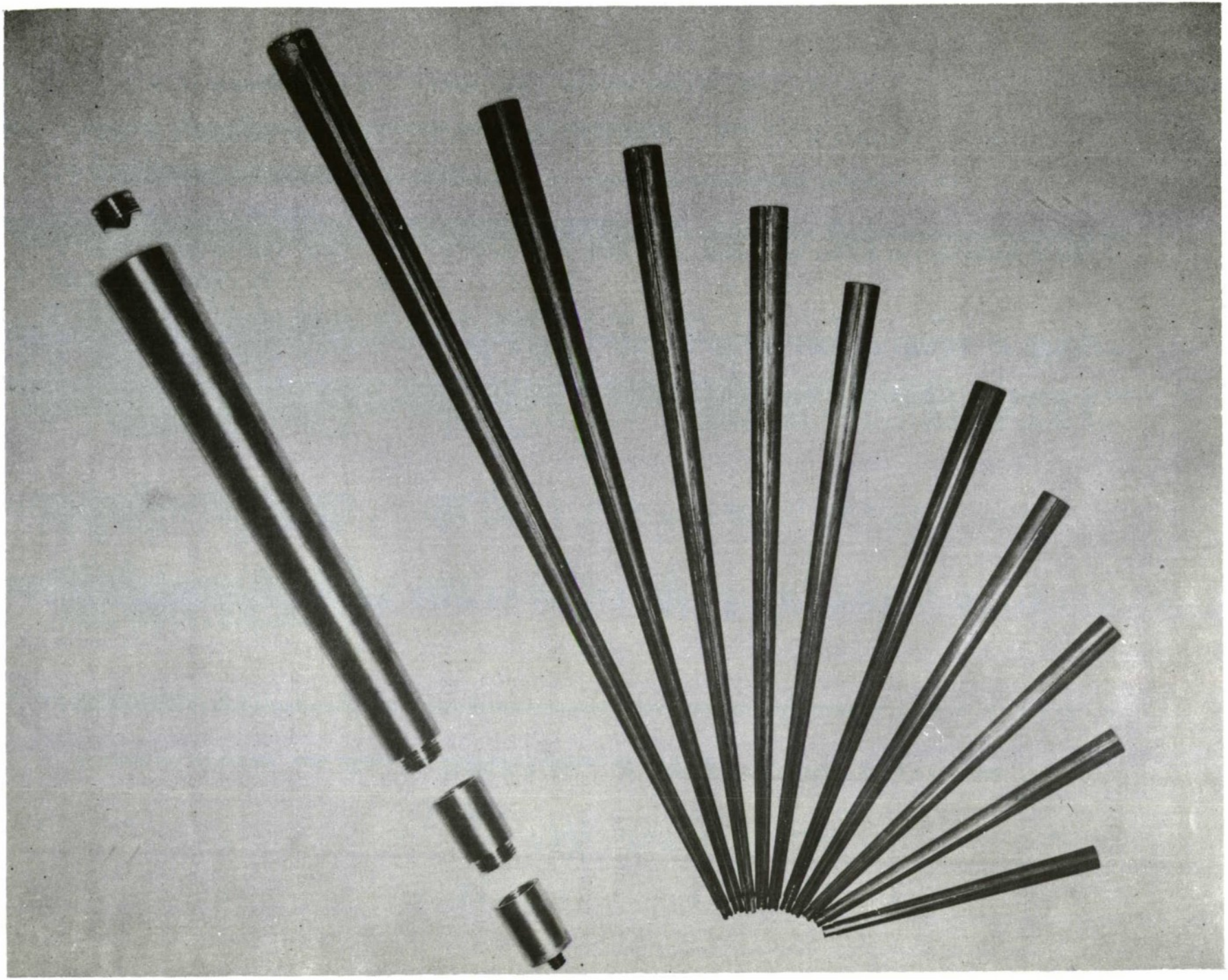

FIG. 1-7 CONICAL ANTENNA WITH STEPWISE VARIATIONS ($\theta_0 = 1.1°$).

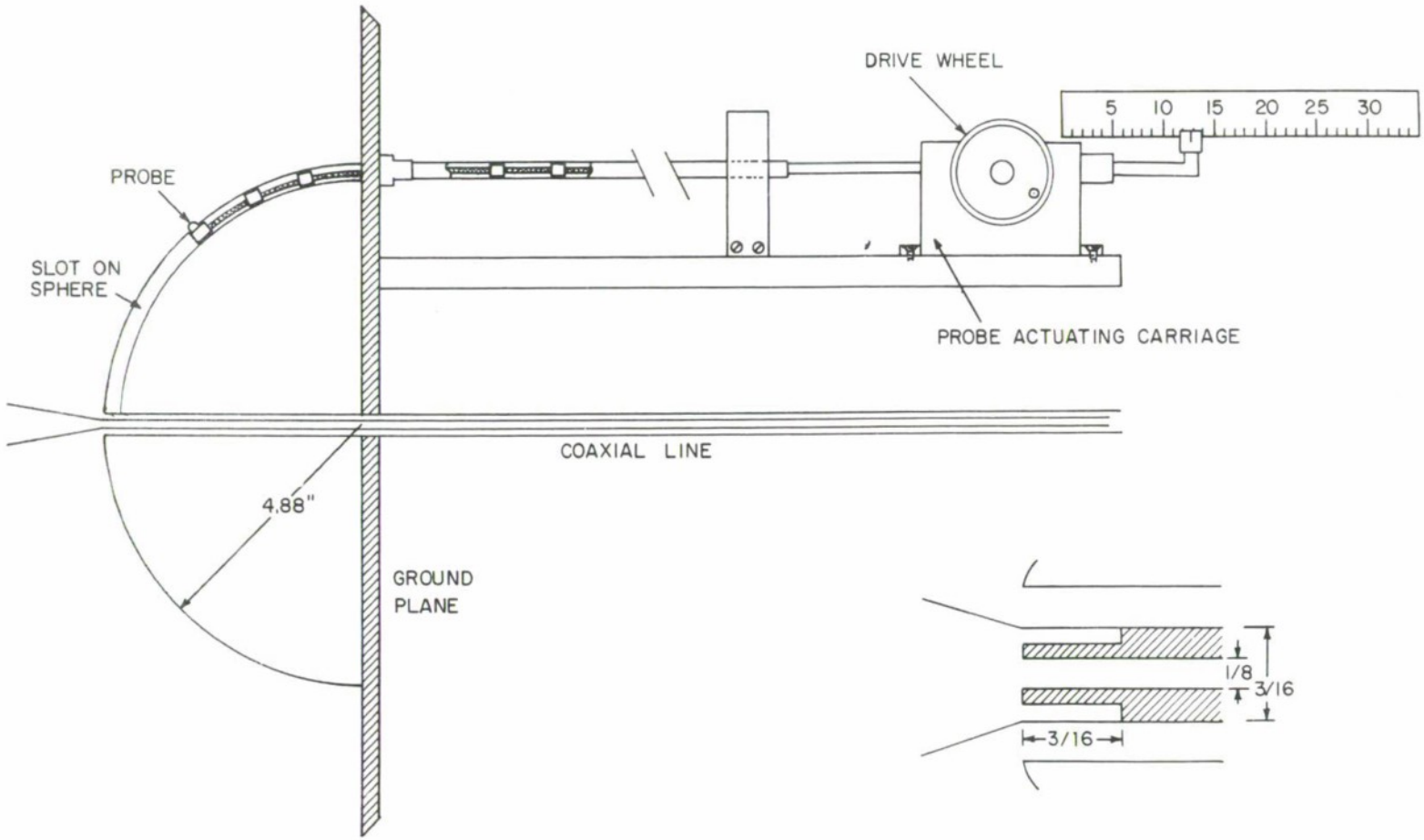

FIG. 1-8 PROBE ON THE HEMISPHERE AND ANTENNA-LINE CONNECTION

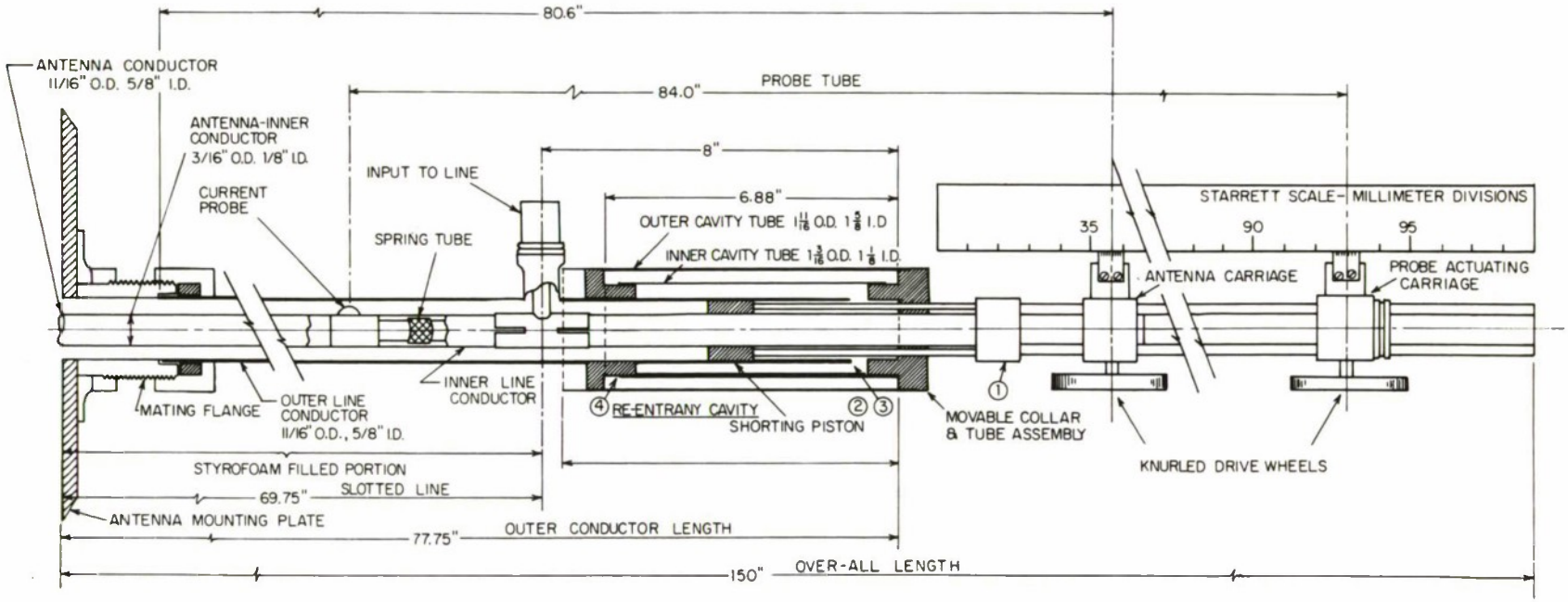

FIG. 1-9 MEASURING LINE DETAILS

plank which is on rollers and a track on top of two 7 ft. long tables.

The dimensions of the line are the result of compromises among the several requirements mentioned earlier. The outer conductor is a brass tube of $\frac{10''}{16}$ (ID); the inner conductor is made of $\frac{3''}{16}$ (OD) brass tubing with a longitudinal slot of width $\frac{1''}{32}$ which extends about 75 in. from the point at which the line penetrates the image plane to the power input connection. The center conductor is positioned by means of a handwheel and rack and pinion mounted behind the main coaxial line. A probe actuating tube of 1/8'' (OD) provides both mechanical and electrical connection to the probes by means of a miniature coaxial cable inside the tube. The probe is also positioned with carriages driven by means of a rack and pinion assembly.

The main coaxial line is completely filled with high density (3.3 lbs./ft.^{3}) expanded polystyrene (''Styrofoam HD-300'') resulting in an electrically and physically continuous structure in which the current and charge distributions are measured in determining a load impedance. Filling the line completely with styrofoam eliminates the difficulties associated with a sagging center conductor or with discontinous dielectric supports. This material is carefully machined for a tight fit inside the outer tube with a sliding fit on the inner tube. A narrow slot was cut into the styrofoam to make room for the probes to enter through the slot in the center conductor.

A desirable feature of the probe system is that it can be used simultaneously for transmission-line measurements and for measuring the current distribution on the attached conical antenna whose probe slot is at a slant angle with the transmission line.

A photograph showing an overall view of current and charge probes is shown in Fig. 1-10. Instead of attaching the probe directly to the probe actuating tube, a section of miniature cable is used between them to enable the probe to traverse the bent antenna. Some difficulty was experienced with this flexible part of the probe system as it moved inside the coaxial line. There was a quite unpredictable twisting or side-motion of this part and this caused some intermittent irregularities in the

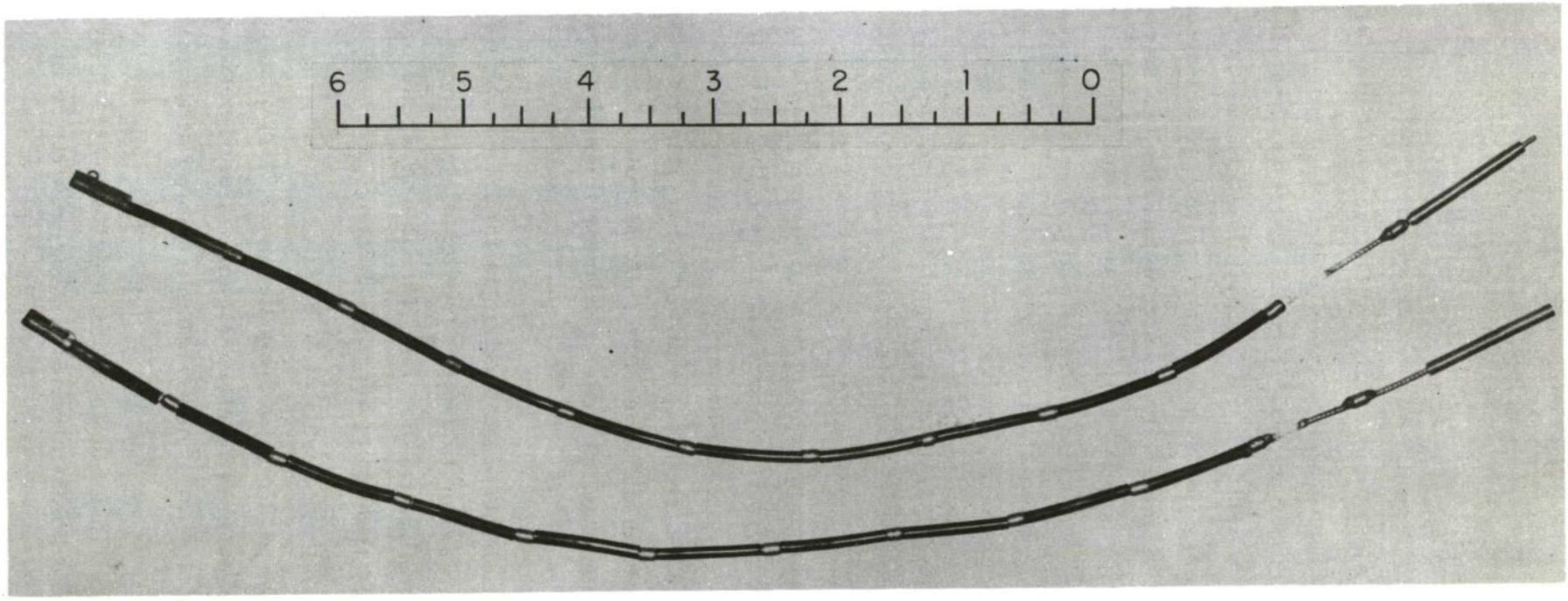

FIG. 1-10 CURRENT AND CHARGE PROBES

distribution measurements in the line and the antenna. The difficulty was solved by the installation of a series of thin tubular springs, a little smaller than the inside diameter of the center conductor, and attached to the miniature coaxial cable with sections of plastic tube as spacer between them. In this manner sufficient flexibility to permit passage through the junction of antenna and transmission line was combined with the strength needed to withstand either compression or extension without noticeable change in length. Another versatile feature of the probe system is the interchangeability of current and voltage probes for transmission-line measurements. Due to the smallness of the inner conductor, the available microdot connection could not be fitted into the center conductor. A specially designed connection was prepared to connect the miniature coaxial line with the probe actuating tube.

Power is fed to the measuring line through a coaxial input connector whose inner conductor makes a sliding contact with the 3/16'' tube. The back cavity, i.e., the section of line behind the feed point should be $\lambda/4$ to present as high a shunting impedance as possible. Since at the lowest operating frequency the cavity would have had to be as much as 75 cms long and this would require an increase in the overall length of the line and probe transverse assembly too great to be accommodated in the available space, a modified so-called re-entrant cavity [20] was used. This allowed the internal distance from the line feed point to the ultimate short circuit in the back-cavity to be effectively increased. This was accomplished by sliding the short-circuiting piston (2) (see Fig. 1-9) to the right, thus continuously increasing the length of the back-cavity until it is stopped by the movable collar and tube assembly. Further motion toward the right will successively open the circuit at (3) and (4). The outer cavity tube (1-11/16'' OD) remains in sliding contact with the fixed collar at (4). This device, when fully extended, essentially triples the length of the back-cavity.

(B) Electrical Properties

Coaxial lines are among the most commonly used for all transmission lines especially at higher frequencies. This is largely because of the

convenient construction and practically perfect shielding between fields inside and outside of the line. The coaxial measuring line is characterized by its characteristic impedance, Z_c, its phase constant β and its attenuation constant α.

These constants may be evaluated from the circuit parameters of a unit length of an infinite line [22].

$$\ell^e = \frac{\mu}{2\pi} \ln(a_2/a_1) \tag{1-114a}$$

$$c = 2\pi\epsilon/\ln(a_2/a_1) \tag{1-114b}$$

$$g = 2\pi\sigma/\ln(a_2/a_1) \tag{1-114c}$$

$$Z^i = \frac{1+j}{2\pi}\left(\frac{\omega\mu_c}{2\sigma_c}\right)^{\frac{1}{2}}\left(\frac{1}{a_1} + \frac{1}{a_2}\right) \tag{1-114d}$$

$$Z_c = \left[(Z^i + j\omega\ell^e)/(g + j\omega c)\right]^{\frac{1}{2}} \tag{1-114e}$$

The several quantities in (1-114a)-(1-114e) are the external inductance, the capacitance, the leakage conductance and the internal impedance per unit length and the characteristic impedance of the infinite line. In these formulae a_1 and a_2 are the inner and outer radii of the coaxial line conductors which have the permeability μ_c, and conductivity σ_c. For the line described in the preceding section, the tubular conductors are brass with $\mu_c = \mu_o$ and with $\sigma_c = 1.29 \times 10^7$ mhos/m. The average measured λ_ℓ (sec. 5) was found to be $\lambda_o/\lambda_\ell = 1.0365$ i. e., $\epsilon_\ell = 1.0744$. Accordingly, from (1-114)

$$\ell^e = 2.408 \times 10^{-7} \quad \text{henry/meter} \tag{1-115a}$$

$$c = 0.046 \times 10^{-9} \quad \text{farad/meter} \tag{1-115b}$$

and the characteristic impedance for a low-loss line can be written approximately as

$$Z_c = 69.07\left(1 - j\frac{r^i}{2\omega\ell^e}\right) \tag{1-116}$$

4. IMAGE SCREEN

For the measurement of current distributions and driving-point admittances of the antenna, a metallic image plane was used so that the observer and the equipment were completely shielded from the field due to the antenna under test. The existing image screen, which is 17 x 20 ft., is attached to the side of Cruft Laboratory. A small number of radial conductors, being distributed as uniformly as possible, are added to the screen to extend the effective size of the existing screen by approximately a factor of two. The detailed structure of this image screen and the additional attached conductors can be found described in Andrew's [18] and Simpson's [20] work. They used the image plane for an experimental study of the dipole at 600 MHz and the top-loaded antenna at 50-250 MHz.

For purposes of assessing the adequacy of the image screen for the present experiment, the input admittances of ordinary brass monopole antennas with lengths 55 cm and 20 cm were measured over the frequencies of interest (100-600 MHz). The lengths chosen correspond approximately to the extreme sizes of the modified antenna to be measured. The results of the measurements are shown in Fig. 1-11 and are found to be in good agreement with both the theoretical and experimental data obtained by others.

It is felt that this test gives a good indication of the usefulness of this image screen for experimental measurements on the modified conical antenna in the frequency range of 100 MHz-600 MHz.

5. ADMITTANCE AND CURRENT DISTRIBUTION MEASUREMENTS

A block diagram of the experimental equipment appears in Fig. 1-12, and a photograph showing the measuring set up is shown in Fig. 1-13. Great simplification resulted from the use of a Hewlett-Packard Model 8405 Vector Voltmeter which replaced the conventional superheterodyne system in which a local oscillator, a mixer and an I-F amplifier and detector are needed for admittance measurements and an additional phase

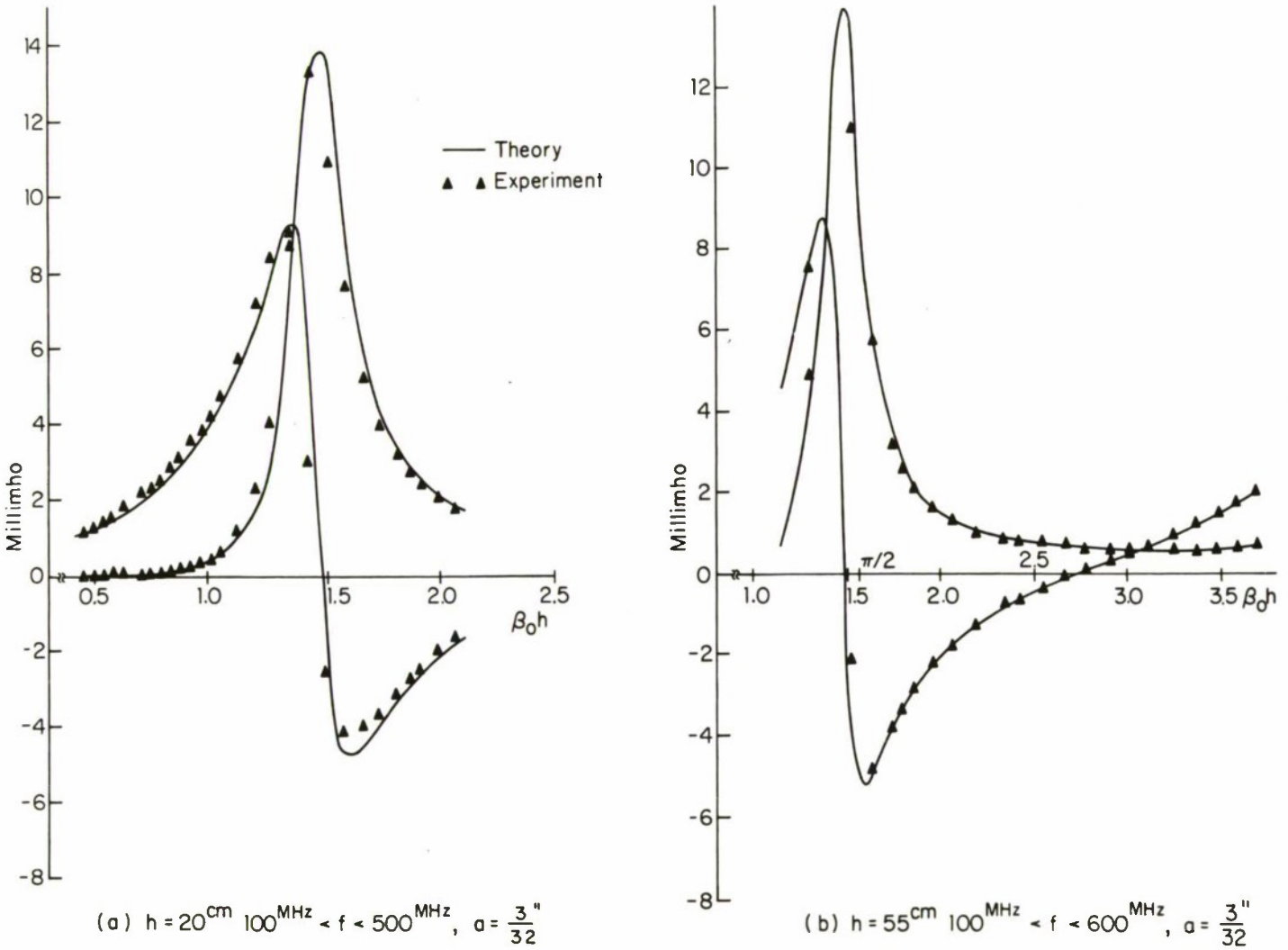

(a) $h = 20^{cm}$ $100^{MHz} < f < 500^{MHz}$, $a = \frac{3''}{32}$

(b) $h = 55^{cm}$ $100^{MHz} < f < 600^{MHz}$, $a = \frac{3''}{32}$

FIG. 1-11 INPUT ADMITTANCE OF MONOPOLE BRASS ANTENNA AT DIFFERENT FREQUENCIES

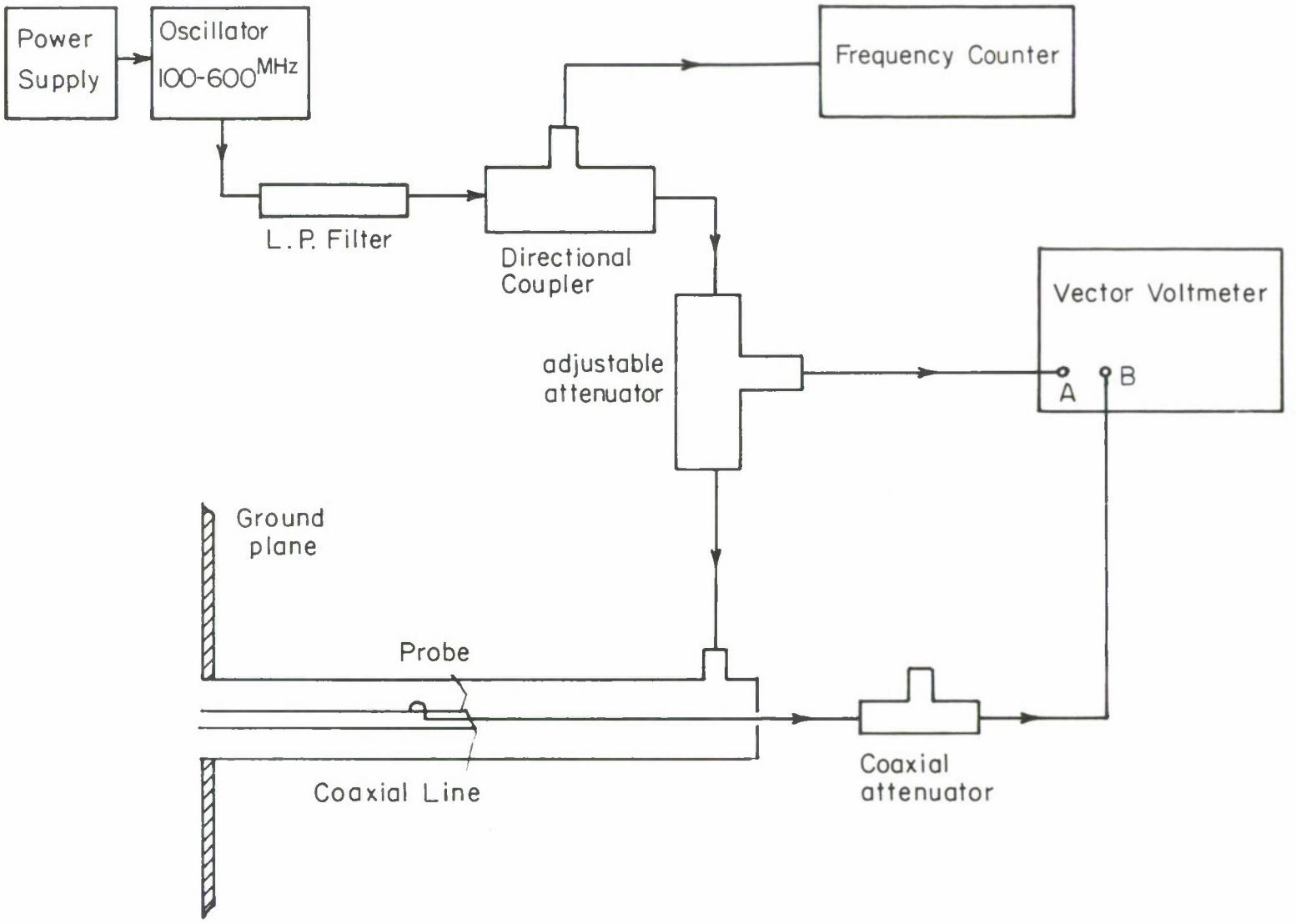

FIG. 1-12 BLOCK DIAGRAM OF THE EXPERIMENTAL SET-UP

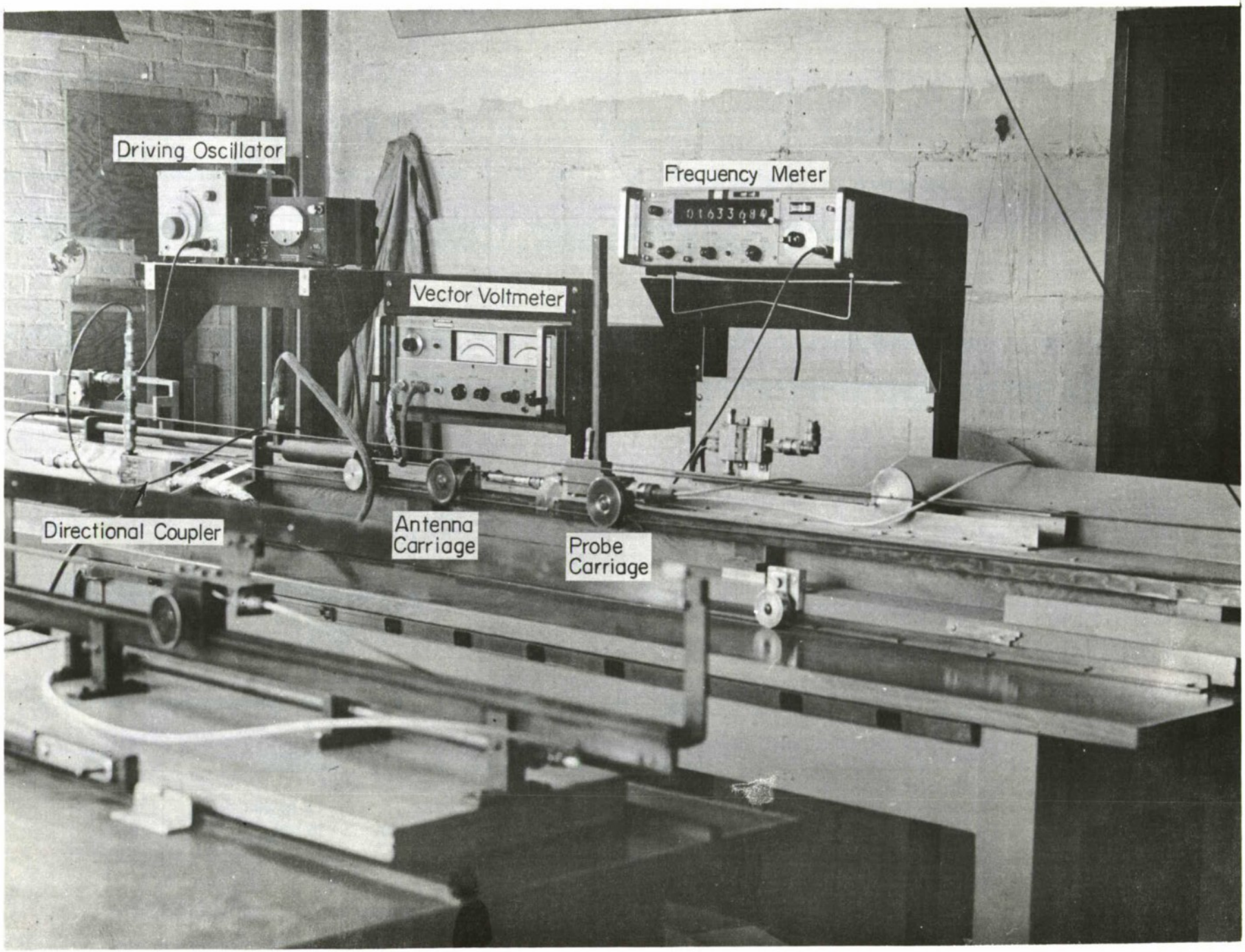

FIG. 1-13 MEASURING LINE AND ASSOCIATED EQUIPMENT

reference line and coaxial hybrid junction are required for current distribution measurements. Basically, the vector voltmeter converts two RF signals of the same fundamental frequency from 1 to 1000 MHz to two 20-KHz IF signals. The IF signals retain the same amplitude wave forms and phase relationship. Consequently, the fundamental components of IF signal have the same amplitude and phase relationship as the fundamental components of RF signals. Accordingly, a small part of the driving voltage is fed to channel A of the vector voltmeter to serve as a reference signal both for amplitude and phase measurements, while the output of a charge or current probe is fed to channel B. The amplitude and phase of the current or charge along either the transmission line or the antenna can be read directly from the vector voltmeter with channel A as reference.

The practical maximum length of the coaxial measuring line is about 2 meters in which the useful range of traverse of the probe is estimated to be somewhat less than 1 meter, the additional length being required to feed the line and to avoid regions of field distortion near discontinuities. The difficulty that the available probe traverse is less than $\lambda/2$ at the lower frequencies (< 150 MHz) can be resolved by the interchange of current and charge probes. With this expedient a quarter wavelength traverse is sufficient.

The dielectric constant of the styrofoam was determined using a known frequency for the input signal (a precision electronic counter Hewlett Packard 4425L was used to measure the frequency of the driving oscillator). The wavelength in the line was measured over a range of frequencies at which at least two nulls were observable by obtaining the distance between the sharp minima resulting from the use of a short circuit on the line. With the frequency and line wavelength known, the velocity of propagation was easily computed. This varies inversely as the square root of the dielectric constant. An average of the measured results yielded $\lambda_o/\lambda_\ell = 1.0365$, i.e., $\epsilon_\ell = 1.0744$.

6. RESULTS

(A) Input Admittance

Due to technical reasons, the conical antenna was prepared with fixed stepwise variation in length and the limited size of the image plane imposed a restriction on the antenna length. Accordingly, the experimental data obtained for the input admittance over the range of operating frequencies (Table 1) do not cover the whole range of antenna lengths ($\beta_0 h = 0.6$ to 3.9), e.g., for $\beta_0 b$ smaller than 0.4 the available data fall mainly in the region of the first resonant antenna length while for $\beta_0 b > 1.11$ the available data are shifted toward the region of antiresonant length. Furthermore, an increase in the operating frequency electrically lengthens the stepwise variation. Therefore, at the higher frequencies, the data points become so sparsely distributed that they can only provide point checks for the theoretical curves.

Frequency MHz	$\beta_0 b$	$(\beta_0 h)_{min}$	$(\beta_0 h)_{max}$
119.37	0.31	0.6	1.5
157.87	0.41	0.6	1.98
196.38	0.51	0.6	2.5
273.39	0.71	0.6	3.44
350.40	0.91	0.75	4.0
388.90	1.01	0.81	4.0
431.68	1.11	0.9	4.0
504.40	1.31	1.06	4.0
581.43	1.51	1.22	4.0

Table 1. Operating Frequencies

Measurements of the input admittance were taken within the frequency range of 100-600 MHz. In Table 1 are listed the actual operating frequencies used in the experiments, the corresponding electrical size of the central sphere, and the range of antenna lengths for which data were taken.

Measured admittances are compared in Fig. 1-14 with the numerical values obtained and presented in Volume II. The experimental data can readily be compared with the theoretical results given in Volume II in which the admittance is defined at the terminals of a single generator of half the symmetric structure erected vertically on an infinite conducting plane. Good agreement is obtained between the measured and theoretical admittances for all ranges of $\beta_0 h$ and $\beta_0 b$, except, perhaps, when h is long and possibly extended too far out from the ground plane. It is also more difficult to center the antenna along the common axis.

Since the input admittance is derived from the standing-wave distribution of the current away from the driving point, the effect of the higher modes at the open end is included in the calculation. As a consequence, the input admittance thus obtained is the apparent admittance in the coaxial line looking toward antenna, and not the exact input admittance defined at the driving point. King [1] has shown that when a coaxial transmission line is connected directly to a cylindrical antenna over an image plane, the principal junction effect can be accounted for by the addition of a small negative capacitance, $-C_T$, which has been determined approximately for cases of interest. Thus, uniform transmission-line theory can be used to define the apparent terminal admittance, Y_{sa}, and by the addition of a terminal-zone correction, $-j\omega C_T$, the terminal admittance Y_0 can be determined. For the modified biconical antenna, approximately the same end correction would be expected as for a simple cylindrical monopole provided the cone angle and b/a are small. No attempt has been made here to determine the effect of the antenna shape upon the end correction.

The value of $-C_T$ for a cylindrical antenna was obtained from Fig. 38.19 of Ref. [1] which gave for $b/a = 0.33$

$$C_T = -0.23 \text{ picofarads}$$

In practice, the correction was almost negligible; for example, at a frequency of 300 MHz

$$B_T = -j\omega C_T = -j0.076 \text{ mmhos}$$

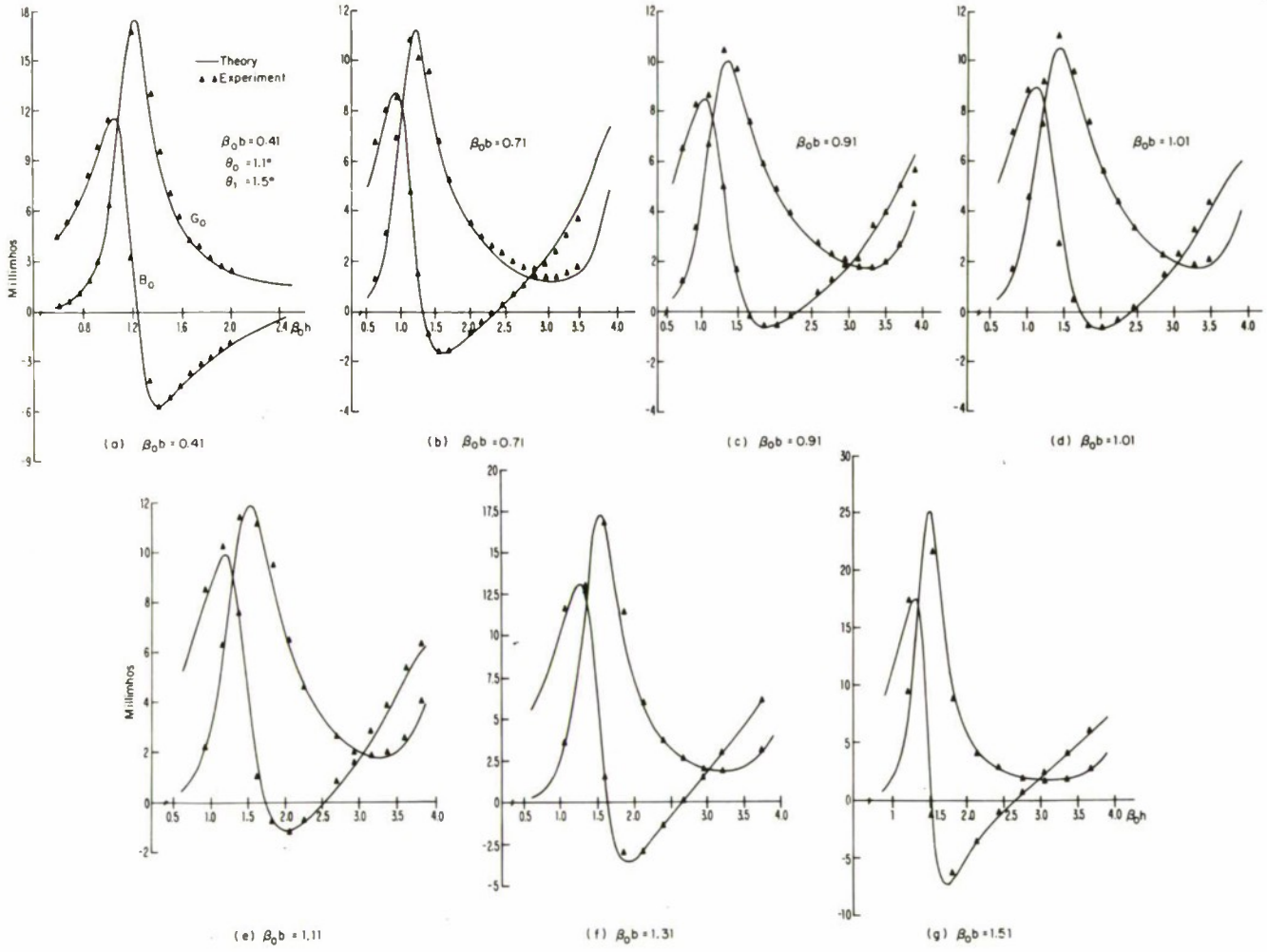

FIG. 1-14 THEORETICAL AND MEASURED ADMITTANCE OF MODIFIED CONICAL ANTENNA VS. ANTENNA LENGTH.

Thus, except in those cases involving exceedingly small values of susceptance, the influence of the terminal-zone correction was almost negligible.

It was observed that virtually no end correction was needed for the measured susceptances.

The fact that very good agreement has been obtained for those extreme sizes of the radiating structure (i.e., $\beta_0 b = 1.51$ and $\beta_0 h = 3.9$) suggests that the restrictions imposed upon the present numerical analysis and computer program are far too conservative and that the computer program can be readily used for modified dipoles of larger size.

(B) Current Distribution

The measured current distributions of selected antennas and central spheres are shown plotted on the same graph in Fig. 1-15 together with the theoretical results. Primarily the longest antenna (h = 35 cms) was used in the current distribution measurement, since it provided antennas ranging from $\beta_0 h = 1.0$ to 3.2 with corresponding central spheres ranging from $\beta_0 b = 0.4$ to 1.2.

In order to obtain an absolute current density distribution instead of a relative one, the experimental values for the antenna are normalized with respect to the apparent admittance and the circumference of the inner conductor, i.e., $Y_{sa}/(2\pi b \sin \theta_0)$. Since it is difficult to move the probe close enough to the edge of the driving gap, the current density on the sphere was normalized with respect to the theoretical value at an angle 12.22° from the axis.

The agreement between the theoretical and experimental curves is quite satisfactory. It is found that the agreement is better for the phase than for the magnitude of the current.

(C) Comparison of Modified Conical and Cylindrical Antennas

The fact that very good agreement has been obtained between the theoretical and experimental results for the modified conical dipole

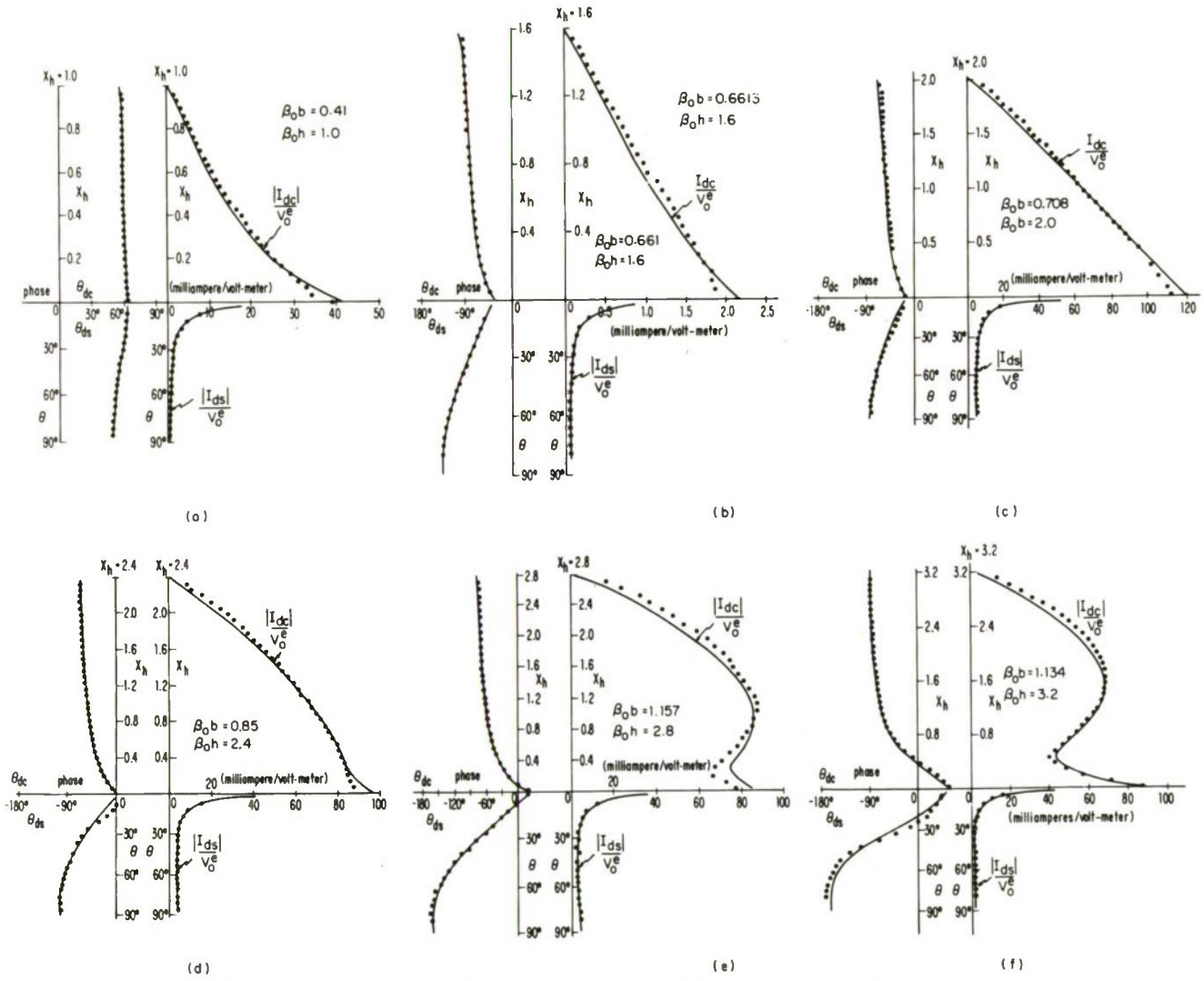

FIG. 1-15 THEORETICAL AND MEASURED CURRENT DISTRIBUTION OF MODIFIED CONICAL ANTENNA

justifies in the first place the analytic formulation presented earlier in this volume and the accuracy of the computed results given in Volume II and secondly equips one with a rather general tool for understanding the performance of modified dipoles in general. To assess the validity of replacing a thin cylindrical antenna by a conical one in the preceding theoretical treatment, a comparison of the measured admittances of modified dipoles with either conical or cylindrical protrusion is made with its length $\beta_0 h$ defined in the conventional way (i.e., for a conical antenna, the length is measured along the radial direction from the driving-point up to the edge of the antenna; while for the cylindrical antenna, it is measured along the axis from the driving-point up to the tip of the hemispherical cap).

In Fig. 1-16 are shown the comparisons of the measured admittances of modified conical and cylindrical antennas for $\beta_0 b = 0.51$, 0.71, 0.91, and 1.01. In general, both curves are of comparable magnitude and nearly the same shape except for a slight shift in $\beta_0 h$. The measured curves for cylindrical protrusion are consistently shifted to the right of those for conical protrusion. This means that the conical protrusion behaves like the cylindrical one with a slightly greater effective antenna length.

The discrepancy between the admittance curves is partially due to the definition of antenna length in which the end cap of the conical antenna is excluded. Therefore, in order to take the end cap into account, it is more suitable to define the antenna length as the actual length along which the current flows; in this way, the end cap will provide an extra antenna length Δh for the conical antenna, namely,

$$\Delta h = \beta_0 a \theta_0 \qquad (1\text{-}117)$$

Accordingly, for $\beta_0 b = 1.01$, Δh ranges from 0.02 to 0.07 with $\beta_0 h$ ranging from 0.0 to 3.5. The end cap effect just described is evident in the results shown in Fig. 1-16 by looking at a special case of $\beta_0 b = 1.01$. The measured admittance of cylindrical protrusion is shifted from that for conical protrusion by approximately 0.08, which is of the same order of magnitude as Δh.

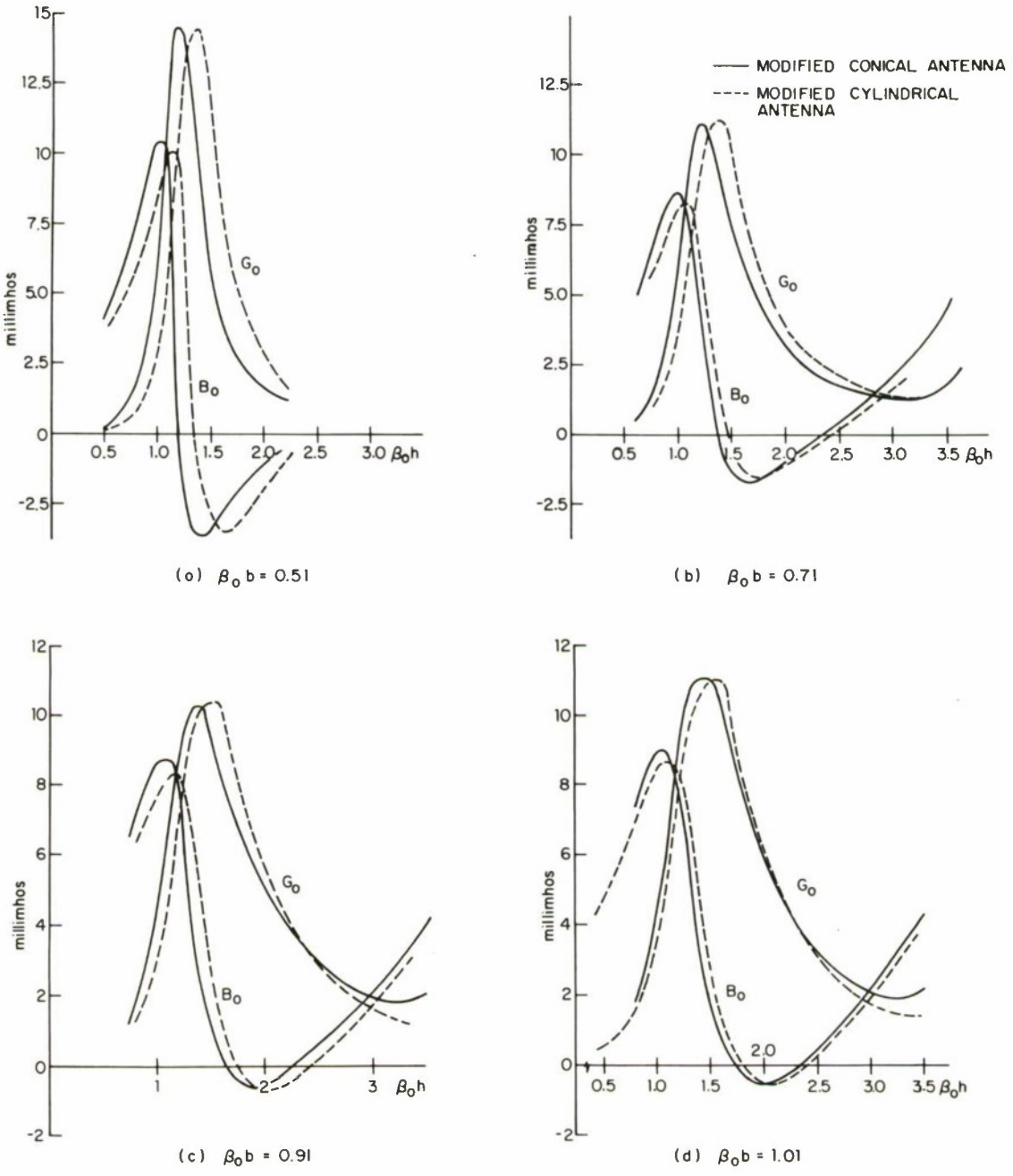

FIG. 1-16 COMPARISON OF MODIFIED CONICAL AND CYLINDRICAL ANTENNA

Another possible reason which might be ascribed to the shift of measured admittances is the fact that in the experimental set-up, the cylindrical antenna has a radius which is the same size as the smaller end of the corresponding conical antenna. This means that on the average the conical antenna should behave like a thicker antenna which tends to have shorter resonant antenna length.

Therefore, after accounting for the end cap effect and thickening effect of conical antennas, a close correspondence of the results for modified dipoles with conical and cylindrical protrusion is accomplished. This means that the assumptions in the theoretical formulation are fairly well supported by the experimental results.

APPENDIX A

INTEGRALS OF PRODUCTS OF LEGENDRE FUNCTION

Let r and k denote integral numbers and v and p non-integral ones. The following integrals of products of Legendre functions exist [2]:

$$\int_0^{\pi} P_k(\theta)\, P_r(\theta) \sin\theta \, d\theta = 0 \qquad (k \neq r) \qquad \text{(A-1)}$$

$$\int_0^{\pi} P'_k(\theta)\, P'_r(\theta) \sin\theta \, d\theta = 0 \qquad (k \neq r) \qquad \text{(A-2)}$$

and

$$J_{kk} = \int_0^{\pi} P_k^2(\theta) \sin\theta \, d\theta$$

or

$$= \frac{1}{k(k+1)} \int_0^{\pi} [P'_k(\theta)]^2 \sin\theta \, d\theta$$

$$= \frac{2}{2k+1} \qquad \text{(A-3)}$$

$$\int_{\theta_0}^{\pi-\theta_0} L_v(\theta)\, L_p(\theta) \sin\theta \, d\theta = 0 \qquad (v \neq p) \qquad \text{(A-4)}$$

$$\int_{\theta_0}^{\pi-\theta_0} L'_v(\theta)\, L'_p(\theta) \sin\theta \, d\theta = 0 \qquad (v \neq p) \qquad \text{(A-5)}$$

$$J_{vv} = \int_{\theta_0}^{\pi-\theta_0} [L_v(\theta)]^2 \sin\theta \, d\theta$$

or

$$= \frac{1}{v(v+1)} \int_{\theta_0}^{-\theta_0} [L'_v(\theta)]^2 \sin\theta \, d\theta$$

$$= \frac{2(1-\mu_0^2)}{2v+1} \left[\frac{\partial L_v(\mu)}{\partial v} \quad \frac{\partial L_v(\mu)}{\partial \mu} \right]_{\mu=\mu_0} \qquad \text{(A-6)}$$

$$J_{vk} = \int_{\theta_0}^{\pi-\theta_0} L_v(\theta) \, P_k(\theta) \sin\theta \, d\theta$$

or

$$= \frac{1}{k(k+1)} \int_{\theta_0}^{-\theta_0} L'_v(\theta) \, P'_k(\theta) \sin\theta \, d\theta$$

$$= \frac{2(1-\mu_0^2)}{[k(k+1) - v(v+1)]} \, P_k(\mu_0) \, L'_v(\mu)\big|_{\mu=\mu_0} \qquad \text{(A-7)}$$

APPENDIX B

BESSEL'S FUNCTIONS

Wronskian

$$M_v(x)\, J'_v(x) - J_v(x)\, M'_v(x)$$

$$= x(j_v + x\, j'_v)(n_v - \eta_v\, j_v) - x\, j_v[(n_v - \eta_v\, j_v) + (n'_v + \eta_v\, j'_v)]$$

$$= -1 \qquad \text{(B-1)}$$

For computational purposes, the following equations exist for large order v:

Define:

$$x_b = v \operatorname{sech} a_b\,, \qquad x = v \operatorname{sech} a \qquad \text{(B-2)}$$

$$J_v(v \operatorname{sech} a) \approx \frac{\exp[v(\tanh a - a)]}{(2\pi v \tanh a)^{1/2}} \Delta J_v \qquad \text{(B-3)}$$

$$J'_v(v \operatorname{sech} a) \approx \left(\frac{\sinh 2a}{4\pi v}\right)^{1/2} \exp[v(\tanh a - a)]\, \Delta J'_v \qquad \text{(B-4)}$$

$$Y_v(v \operatorname{sech} a) \approx \frac{\exp[v(a - \tanh a)]}{(\pi v \tanh a/2)^{1/2}} \Delta Y_v \qquad \text{(B-5)}$$

$$Y'_v(v \operatorname{sech} a) \approx \left(\frac{\sinh 2a}{\pi v}\right)^{1/2} \exp[v(a - \tanh a)]\, \Delta Y'_v \qquad \text{(B-6)}$$

where

$$\Delta J_v = 1 + \sum_{k=1}^{\infty} \frac{U_k(\coth a)}{v^k} \qquad \text{(B-7)}$$

$$\Delta J'_v = 1 + \sum_{k=1}^{\infty} \frac{V_k(\coth a)}{v^k} \qquad \text{(B-8)}$$

$$\Delta Y_v = 1 + \sum_{k=1}^{\infty} (-1)^k \frac{U_k(\coth a)}{v^k} \qquad (B-9)$$

$$\Delta Y'_v = 1 + \sum_{k=1}^{\infty} (-1)^k \frac{V_k(\coth a)}{v^k} \qquad (B-10)$$

Therefore,

$$J'_v(x) = \left(\frac{\pi}{2x}\right)^{1/2} J_v(x)\left(1/2 + x \sinh a \frac{\Delta J'_v}{\Delta J_v}\right) \qquad (B-11)$$

$$M_v(x) = N_v(x) - \frac{\hat{N}'_v(x_b)}{J'_v(x_b)} \hat{J}_v(x)$$

$$= (\pi x/2)^{1/2} Y_v(x_b)(\tanh a_b/\tanh a)^{1/2} \cdot$$

$$-\Delta_b \exp(v\ ) \frac{\Delta J_v(x)}{\Delta J_v(x_b)} + \exp(-v\ ) \frac{\Delta Y_v(x)}{\Delta Y_v(x_b)} \qquad (B-12)$$

$$M'_v(x) = (\pi/2x)^{1/2} Y_v(x_b)\left[1/2 + x \sinh a \frac{\Delta J'_v(x)}{\Delta J_v(x)}\right] \cdot$$

$$\left[-\Delta_b \exp(v\ ) + \Delta_x \exp(-v\ )\right] \left[\frac{\tanh a_b}{\tanh a}\right]^{1/2} \qquad (B-13)$$

where

$$\Delta_x = \frac{\left[1/2 - x \sinh a\, \Delta Y'_v(x)/\Delta Y_v(x)\right]}{\left[1/2 + x \sinh a\, \Delta J'_v(x)/\Delta J_v(x)\right]} \qquad (B-14)$$

$$\Delta_b = \frac{\left[1/2 - x_b \sinh a_b\, \Delta Y'_v(x_b)/\Delta Y_v(x_b)\right]}{\left[1/2 + x_b \sinh a_b\, \Delta J'_v(x_b)/\Delta J_v(x_b)\right]} \qquad (B-15)$$

$$= a_b - a - \tanh a_b - \tanh a \qquad (B-16)$$

REFERENCES

1. R. W. P. King, "The Theory of Linear Antenna", Harvard University Press, Cambridge, Mass., 1956.

2. R. W. P. King, "The Linear Antenna - Eighty Years of Progress", Proceedings of the IEEE, Vol. 55, No. 1, pp. 2-15, January 1967.

3. C. H. Papas and R. King, "Surface Currents on a Conducting Sphere Excited by a Dipole", Journal of Applied Physics, Vol. 19, No. 9, pp. 808-816, September 1948.

4. K. Iizuka, "An Experimental Study of a Monopole over a Grounded Hemisphere", IEEE Trans. Antenna and Propagation, Vol. AP-16, pp. 764-766, Nov. 1968.

5. F. M. Tesche and A. R. Neureuther, "Radiation Pattern for Two Monopoles on Perfectly Conducting Sphere", IEEE Trans. Antenna and Propagation, Vol. AP-18, pp. 692-694, September 1970.

6. S. A. Schelkunoff, "Theory of Antennas of Arbitrary Size and Shape", Proc. IRE, Vol. 29, pp. 493-521, 1941.

7. S. A. Schelkunoff, "Principal and Complementary Waves in Antenna", Proc. IRE, Vol. 34, pp. 23-32, 1946.

8. S. A. Schelkunoff, "General Theory of Symmetrical Biconical Antenna", J. Appl. Phys., Vol. 22, pp. 1330-1332, Nov. 1951.

9. C. T. Tai, "On the Theory of Biconical Antenna", J. Appl. Phys., Vol. 19, pp. 11-23, 1948.

10. C. T. Tai, "A Study of E. M. F. Method", J. Appl. Phys., Vol. 20, pp. 717-723, July 1949.

11. P. D. P. Smith, "The Conical Dipole of Wide Angle", J. Appl. Phys. Vol. 19, pp. 11-23, January 1948.

12. C. H. Papas and R. W. P. King, "Input Impedance of Wide Angle Conical Antennas Fed by a Coaxial Line", Proc. IRE, Vol. 37, pp. 1269-1271, November 1949.

13. D. M. Bolle and M. D. Morganstern, "Monopole and Conical Antenna on Spherical Vehicles", IEEE Trans. Antenna and Propagation, Vol. AP-17, pp. 477-484, July 1969.

14. D. S. Jones, "The Theory of Electromagnetism", Chpts. 1 and 8, The Macmillan Company, N. Y. 1964.

15. A. Erdelyi, "Higher Transcendental Functions", Vol. I, pp. 163-164, McGraw-Hill Book Company, 1953.

16. E. W. Hobson, "The Theory of Spherical and Ellipsoidal Harmico", pp. 399-408, Chelsea Publishing Comp., N. Y., 1955.

17. D. C. C. Chang, "On the Electrically Thick Monopole, Part I - Theoretical Solution, Part II - Experimental Study", IEEE Trans., Vol. AP-16, No. 1, pp. 58-71, January 1968.

18. H. W. Andrews, "The Collinear Antenna Array Theory and Measurements", Tech. Report No. 178, Cruft Lab., Harvard University, Cambridge, Mass., July 1953.

19. D. Mack, "A Study of Circular Arrays - Experimental Equipment", Tech. Report No. 381, Cruft Lab., Harvard University, Cambridge, Mass., May 1963.

20. T. L. Simpson, "Top-Loaded Antennas: A Theoretical and Experimental Study", Ph. D. Thesis Assertion, Harvard University, Cambridge, Mass., June 1969.

21. H. Whiteside, "Electromagnetic Field Probes", Cruft Lab. Tech. Report No. 377, Harvard University, Cambridge, Mass. 1962.

22. R. W. P. King, "Transmission Line Theory", Dover Publications Inc., N. Y., pp. 13-23, 1963.

23. L. D. Scott, "Apparatus for Studying the Properties of Antennas in an Effectively Infinite Dissipative Medium", Tech. Report No. 6, DEAP, Harvard University, Cambridge, Mass., December 1969.

UNCLASSIFIED

Security Classification

DOCUMENT CONTROL DATA – R&D

(Security classification of title, body of abstract and indexing annotation must be entered when the overall report is classified)

1. ORIGINATING ACTIVITY *(Corporate author)*
Harvard University under Purchase Order No. C782 to M.I.T. Lincoln Laboratory

2a. REPORT SECURITY CLASSIFICATION
Unclassified

2b. GROUP
None

3. REPORT TITLE
Modified Dipoles: I. Theoretical and Experimental Study

4. DESCRIPTIVE NOTES *(Type of report and inclusive dates)*
Final Summary Report

5. AUTHOR(S) *(Last name, first name, initial)*
Kao, Peter S.

6. REPORT DATE	7a. TOTAL NO. OF PAGES	7b. NO. OF REFS
July 1971	77	23

8a. CONTRACT OR GRANT NO.
F19628-70-C-0230

b. PROJECT NO.
627A

c.
Purchase Order No. C782

d.

9a. ORIGINATOR'S REPORT NUMBER(S)
Scientific Report No. 13 (Vol. I)

9b. OTHER REPORT NO(S) *(Any other numbers that may be assigned this report)*
ESD-TR 71-246

10. AVAILABILITY/LIMITATION NOTICES
Approved for public release; distribution unlimited.

11. SUPPLEMENTARY NOTES
Vol. II is ESD-TR-72-181

12. SPONSORING MILITARY ACTIVITY
Air Force Systems Command, USAF

13. ABSTRACT

The 'modified dipole' has its origin in the consideration of the general properties of a satellite antenna which bears great resemblance to a dipole modified to incorporate at the center a conducting volume which is used to radiate electromagnetic waves and to house a power supply and radio frequency generators, etc. The object of this research is to pursue a theoretical and experimental exploration of the effects induced by the presence of the conducting volume on the antenna performance, i.e., input characteristics, current distribution along the surfaces of the entire radiating structure and radiation properties.

In Volume I a mathematical model consisting of a perfectly conducting sphere from which project the ends of a thin biconical antenna is chosen to simulate the actual sphere-centered thin dipole. The conical antenna is driven at its junction with the sphere by a rotationally symmetric electric field maintained across the gap by a biconical transmission line excited by the TEM mode. The attractive features of this model include the fact that it has surfaces that permit a simple specification of boundary conditions and, hence, a rigorous formulation for the electromagnetic fields and a shape such that its properties should come reasonably close to those of a modified cylindrical antenna as the cone angle becomes quite small.

The measurements of both input admittances and current distributions on modified dipoles (with either conical or cylindrical antenna projecting from the sphere) are also presented in Volume I. Comparisons were also made between modified conical and cylindrical antennas with the same sphere radii and antenna heights. The radius of the cylindrical antenna is the same as the smaller end of the cone. The fact that the admittance curves for modified cylindrical and conical antennas involve only slight shifts suggests that by introducing an equivalent antenna length that is a little longer than the actual physical length of the conical antenna a good approximation is obtained for the cylindrical antenna.

An infinite set of algebraic equations was solved numerically in Volume II for small cone angles. Comparisons were made between the modified conical antenna and its limiting biconical antenna which provides both an extrapolatory numerical check for the modified conical antenna with shrinking central sphere and an understanding of the underlying physical phenomena. Theoretical and experimental results are in very good agreement.

14. KEY WORDS

Modified dipoles
Conical antennas
Cylindrical antennas
Input admittances
Current distributions

UNCLASSIFIED

Security Classification